Taylor & Francis
Taylor & Francis Group

RESEARCH PAPER

🔓 OPEN ACCESS

Quantitative and predictive model of kinetic regulation by *E. coli* TPP riboswitches

Sondés Guedich[a], Barbara Puffer-Enders[a], Mireille Baltzinger[b], Guillaume Hoffmann[c], Cyrielle Da Veiga[a], Fabrice Jossinet[d], Stéphane Thore[e], Guillaume Bec[a], Eric Ennifar[a], Dominique Burnouf[a], and Philippe Dumas[a]

[a]IBMC-CNRS, Biophysique et Biologie Structurale, Architecture et Réactivité de l'ARN, Université de Strasbourg, Strasbourg, France; [b]IBMC-CNRS, Régulations post-transcriptionnelles et nutrition, Architecture et Réactivité de l'ARN, Université de Strasbourg, Strasbourg, France; [c]EMBL Grenoble Outstation, Grenoble, France; [d]IBMC-CNRS, Evolution des ARN non codants chez la levure, Architecture et Réactivité de l'ARN, Université de Strasbourg, Strasbourg, France; [e]Université de Bordeaux, Institut Européen de Chimie et Biologie, ARNA laboratory; INSERM-U1212; CNRS-UMR5320; Bordeaux, France

ABSTRACT

Riboswitches are non-coding elements upstream or downstream of mRNAs that, upon binding of a specific ligand, regulate transcription and/or translation initiation in bacteria, or alternative splicing in plants and fungi. We have studied thiamine pyrophosphate (TPP) riboswitches regulating translation of *thiM* operon and transcription and translation of *thiC* operon in *E. coli*, and that of *THIC* in the plant *A. thaliana*. For all, we ascertained an induced-fit mechanism involving initial binding of the TPP followed by a conformational change leading to a higher-affinity complex. The experimental values obtained for all kinetic and thermodynamic parameters of TPP binding imply that the regulation by *A. thaliana* riboswitch is governed by mass-action law, whereas it is of kinetic nature for the two bacterial riboswitches. Kinetic regulation requires that the RNA polymerase pauses after synthesis of each riboswitch aptamer to leave time for TPP binding, but only when its concentration is sufficient. A quantitative model of regulation highlighted how the pausing time has to be linked to the kinetic rates of initial TPP binding to obtain an ON/OFF switch in the correct concentration range of TPP. We verified the existence of these pauses and the model prediction on their duration. Our analysis also led to quantitative estimates of the respective efficiency of kinetic and thermodynamic regulations, which shows that kinetically regulated riboswitches react more sharply to concentration variation of their ligand than thermodynamically regulated riboswitches. This rationalizes the interest of kinetic regulation and confirms empirical observations that were obtained by numerical simulations.

Introduction

Thiamine pyrophosphate (TPP), the active form of thiamine (vitamin B1), is an essential cofactor for many enzymes, particularly in the universally conserved pyruvate dehydrogenase complex involved in the citric acid cycle (or Krebs cycle).[1] As such, cellular TPP concentration has to be tightly regulated. In bacteria, thiamine and TPP are synthesized *de novo* following a complex pathway[2-4] sketched in Fig. 1 for *E. coli*. It has long been considered that the regulation of such a pathway was exclusively protein-dependent. However, non-coding leader regions of mRNA, precisely of mRNAs involved in thiamine biosynthesis, were shown to be important in the regulation process. It was hypothesized that TPP could interact directly with the regulatory sequence,[5] which was shown rapidly to hold true.[6,7] The same scenario had occurred for the interaction of vitamin B12 with the *btuB* mRNA leader.[8-10] Such RNA regulatory modules found in the 5′-UTR of bacterial mRNAs have been coined riboswitches.[8] Since then, many other riboswitches have been uncovered,[11] comprising riboswitches in the 3′-UTR of plant and fungi mRNAs,[12] and structural aspects as well as their modes of action have been reviewed.[13-16] Globally, a riboswitch is divided

into an aptamer domain able to bind its specific ligand and a so-called expression platform. Regulation originates from alternative pairing of sequences in the aptamer domain and in the expression platform depending on the concentration of the ligand (Fig. 2AB).
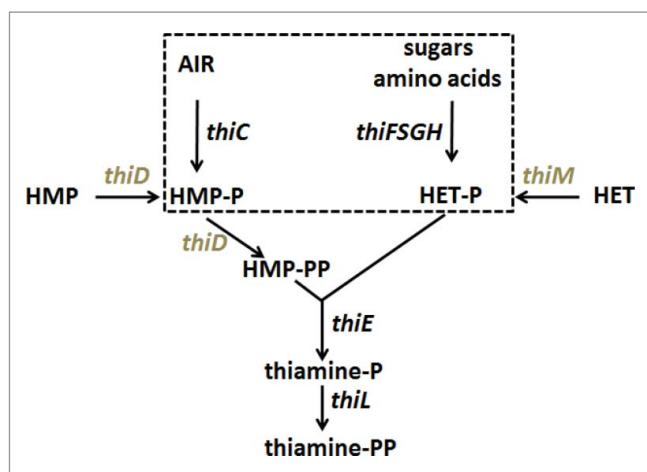
An important aspect concerning the mechanism of action of a riboswitch is whether it is acting thermodynamically, or kinetically. In the first case, the dissociation constant of its specific ligand fits with the cellular concentration of the ligand to be maintained and the mass action law governs the riboswitch response. In the second case, the dissociation constant is too low, *i.e.* the affinity is too high, for a thermodynamic control since the riboswitch would always be saturated by its ligand and, therefore, would never act as a switch. The riboswitch, then, has to proceed by a kinetic mechanism.[17,18] This aspect is particularly important for transcription regulators, because a decision has to be taken 'on the fly' after synthesis of the aptamer sequence, but before the RNA polymerase has reached the critical point after which it cannot be halted anymore. In this particular case of TPP riboswitches, crude measurements

Figure 1. Simplified view of the thiamine biosynthesis pathway in *E.coli*. Enzymes encoded by the *thiC* operon (thiC and thiF,S,G,H, dashed box) synthezise the primary substrates hydroxymethylpyrimidine phosphate (HMP-P) and hydroxyethylthiazole phosphate (HETP). AIR: Amino-imidazole ribotide. Note that *thiE* is in the same operon. Genes in the *thiM* operon (*thiM* and *thiD* in gray) code for kinases that ultimately produce HMP-PP. Adapted from.[3]

of TPP in cells [19,20] allowed us to derive that, depending on the growing media in use, the TPP concentration lies roughly in the range 3-150 μM. In addition, the K_d values of TPP as a cofactor of different bacterial enzymes range from 0.27 to 9 μM with a mean value of 3 μM (SD-1). One may thus consider that riboswitch-mediated regulation, be it of kinetic or thermodynamic nature, has to switch from the OFF to the ON state in response to a concentration of free TPP decreasing (roughly) below the micromolar range.

We have considered in this work three structurally-related, but functionally different TPP riboswitches, two in *E. coli* and one in *A. thaliana* (Fig. 2). *E. coli thiM* riboswitch regulates translation of the *thiM* operon[6,21] (Fig. 1A), whereas genetic control of the *thiC* operon by *E. coli thiC* riboswitch appears to occur both at the level of translation and transcription.[6] For the latter, however, no clear sequence signatures that could explain these properties are apparent.[6] *A. thaliana THIC* riboswitch regulates 3′-UTR processing with alternative splicing events depending upon the TPP concentration [12] (from now on *ECthiC*, *ECthiM* and *ATthiC* will stand respectively for *E. coli thiC, E. coli thiM* and *A. thaliana thiC*). One major difference between these prokaryotic and plant riboswitches is that, in line with their respective functions, *ECthiC* and *ECthiM* are in the 5′-UTR, whereas *ATthiC* is in the 3′-UTR. Also, the expression platform is downstream of the aptamer in *ECthiC* and *ECthiM*, whereas it is upstream of the aptamer in *ATthiC* (Fig. 2AB).

Our goal was to compare their kinetics of folding and, particularly, to fully understand the regulatory mechanism. For that, we have used extensively hydroxyl-radical (•OH) footprinting (with an efficient processing method), which confirmed that the ditopic TPP (Fig. 2C) interacts first within the RNA mostly through its pyrimidine moiety and not through its pyrophosphate. We also used our recently developed kinetic method (*kinITC*) based on Isothermal Titration Calorimetry (ITC)[22] in conjunction with Surface Plasmon Resonance (SPR). We verified that these TPP riboswitches follow a pure 'induced-fit' mechanism involving a first binding step followed by complete RNA folding. Based upon the firmly established

kinetic model, *kinITC* yielded the full set of thermodynamic and kinetic parameters for the two *E. coli* riboswitches, which showed that they are kinetically regulated. A quantitative model linked these experimentally determined parameters to the dependence of *ECthiC-* and *ECthiM*-mediated regulation on TPP concentration. This yielded a regulation curve with a typical sigmoid shape indicating a switch at a TPP concentration in the expected micromolar range. In contrast, the plant riboswitch is thermodynamically regulated and showed considerable dependence of its kinetics of folding upon temperature, which suggests that it could also act as a thermosensor.

Results

Hydroxyl-radical footprinting results: kinetic aspects

Hydroxyl-radical-footprinting experiments were performed on *ATthiC* and on *ECthiC$_{mutP1}$* related to *ECthiC* (Fig. 2D). The results showed that *ATthiC* folds very slowly at room temperature since 30 min were necessary at 25°C to achieve its folding after TPP addition at 2 μM concentration (Fig. 3). Importantly, this slow folding was not due to the low TPP concentration used in this experiment as confirmed by •OH experiments at higher TPP concentrations (not shown) and by kinetic ITC experiments at high TPP concentrations (Fig. SD-2A). This means that, around 25°C, *ATthiC* is intrinsically a slow folder irrespective of the TPP concentration above 0.1 μM (see conclusion of SD-9). In comparison, *ECthiC$_{mutP1}$* achieved its folding at 27°C in less than 10 s (Fig. SD-3ABC). The overall folding process of *ATthiC* showed unambiguously a fast component characterized by a 'short time' (8 ± 2)s and a slow component characterized by a 'long time' (700 ± 140)s (Fig. 3A). Such a behavior is the mark of a kinetic mechanism in two steps, as a single kinetic step with a large excess of ligand (justifying 1st-order approximation) would only show one single exponential time.

Two extreme kinetic models are possible. Kinetic model #1 ('induced fit') implies that the TPP ligand (L) binds to the incompletely folded RNA (R_0) to yield the bound species R_1 subsequently folded fully into R_2 according to the two steps:

$$R_0 + L \underset{k_{off}}{\overset{k_{on}}{\rightleftharpoons}} R_1 \tag{1a}$$

$$R_1 \underset{k_U}{\overset{k_F}{\rightleftharpoons}} R_2 \tag{1b}$$

Alternatively, kinetic model #2 ('conformational selection') implies that the essential folding step occurs first and TPP binding in a second step, according to:

$$R_0 \underset{k_U}{\overset{k_F}{\rightleftharpoons}} R_1 \tag{2a}$$

$$R_1 + L \underset{k_{off}}{\overset{k_{on}}{\rightleftharpoons}} R_2 \tag{2b}$$
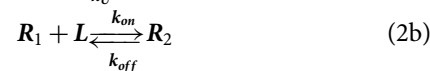
In both cases, k_F and k_U stand, respectively, for 'folding' and 'unfolding' and one may define the dissociation constant $K_d = k_{off} / k_{on}$ and the equilibrium constant $K_F = k_F / k_U$.
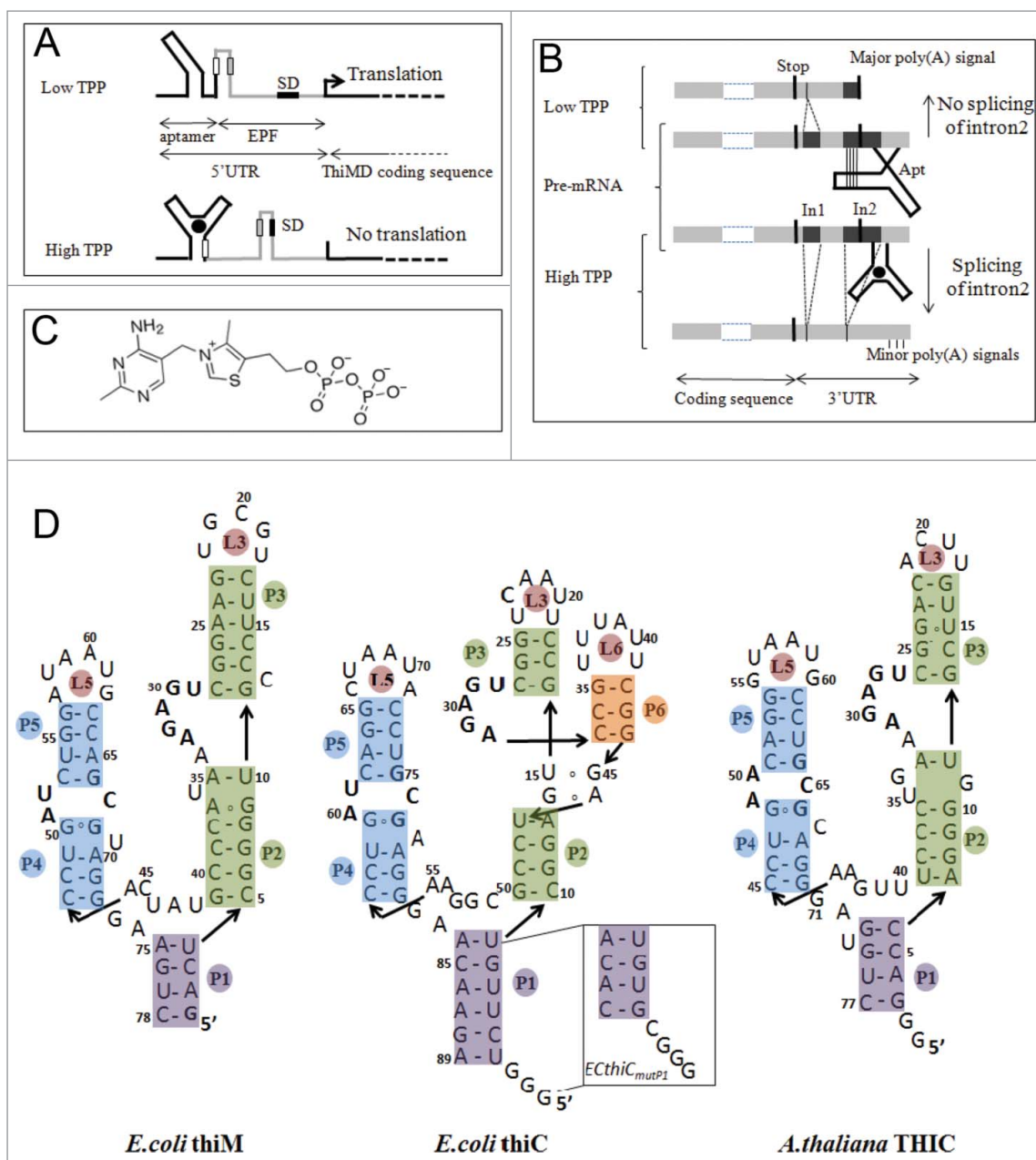
Figure 2 Organization, regulation mechanisms and secondary structures of *E.coli* and *A.thaliana* thiamine pyrophosphate riboswitches. (A) In *E.coli*, riboswitches are located in the 5'-UTR and control translation (*thiM*, shown here as an example) and/or transcription (*thiC*) of the downstream genes. At low TPP concentration, the aptamer (black) is not fully folded and the regulatory sequence (here the Shine-Dalgarno sequence,SD) in the expression platform (EPF, gray) is available for gene expression whereas, at higher concentration, TPP binding induces a sequestering of SD, which prevents initiation of translation see Fig. 8B for *thiC*. (B) In *A.thaliana*, the TPP riboswitch is located in the 3'-UTR of the gene THIC. At low TPP concentration, the 5'-strands of helices P4 and P5 pair within intron 2 (In2), which masks the 5'-splice site, leaves the major poly-adenylation site available and produces a short stable transcript. At higher TPP concentration, the riboswitch aptamer folds completely, which permits Intron 2 splicing and removal of the major poly(A) site thus producing a longer unstable transcript (adapted from [12]). (C) Structure of the ditopic thiamine pyrophosphate with the pyrimidine and pyrophosphate groups interacting at different locations within the RNA (see D). (D) The sequences of the bacterial riboswitch aptamers are the wild type sequences, whereas the sequence of *ATthiC* is the one used for the crystallographic study.[51] The stem P3 is most variable in plant riboswitches and the retained shortened P3 corresponds to the conserved part.[12] The box labeled *ECthiC_{mutP1}* corresponds to the sequence of a P1-helix variant of *ECthiC* (see text). The conserved loop sequence **UGAGA** between P2 and P3 is the binding site for the pyrimidine moiety of the TPP and the conserved internal loop between P4 and P5 is the pyrophosphate binding site.

It is extremely important to emphasize that K_d corresponds to the dissociation constant, either of the initial step (model #1), or of the final step (model #2), **and not** to the overall dissociation constant (noted K_d(overall) in the following). Whatever the kinetic model, the two terms are related by K_d(overall) = K_d / K_F. Keeping in mind this difference between K_d and K_d(overall) is crucial for correct understanding and for a valid comparison with previous works that reported on K_d(overall) [23-25] For example, for *ECthiM*, we obtained at 30°C K_d(overall) = 19 nM, but K_d = 0.45 μM with K_F = 23.3. Thermodynamically, the two models cannot be discriminated since ΔH(overall) = $\Delta H_{Binding}$ + $\Delta H_{Folding}$ and K_d(overall) = K_d / K_F are equally verified in the two situations. However, the two models can be discriminated kinetically. The mathematical basis for this discrimination is explained in Materials and Methods.
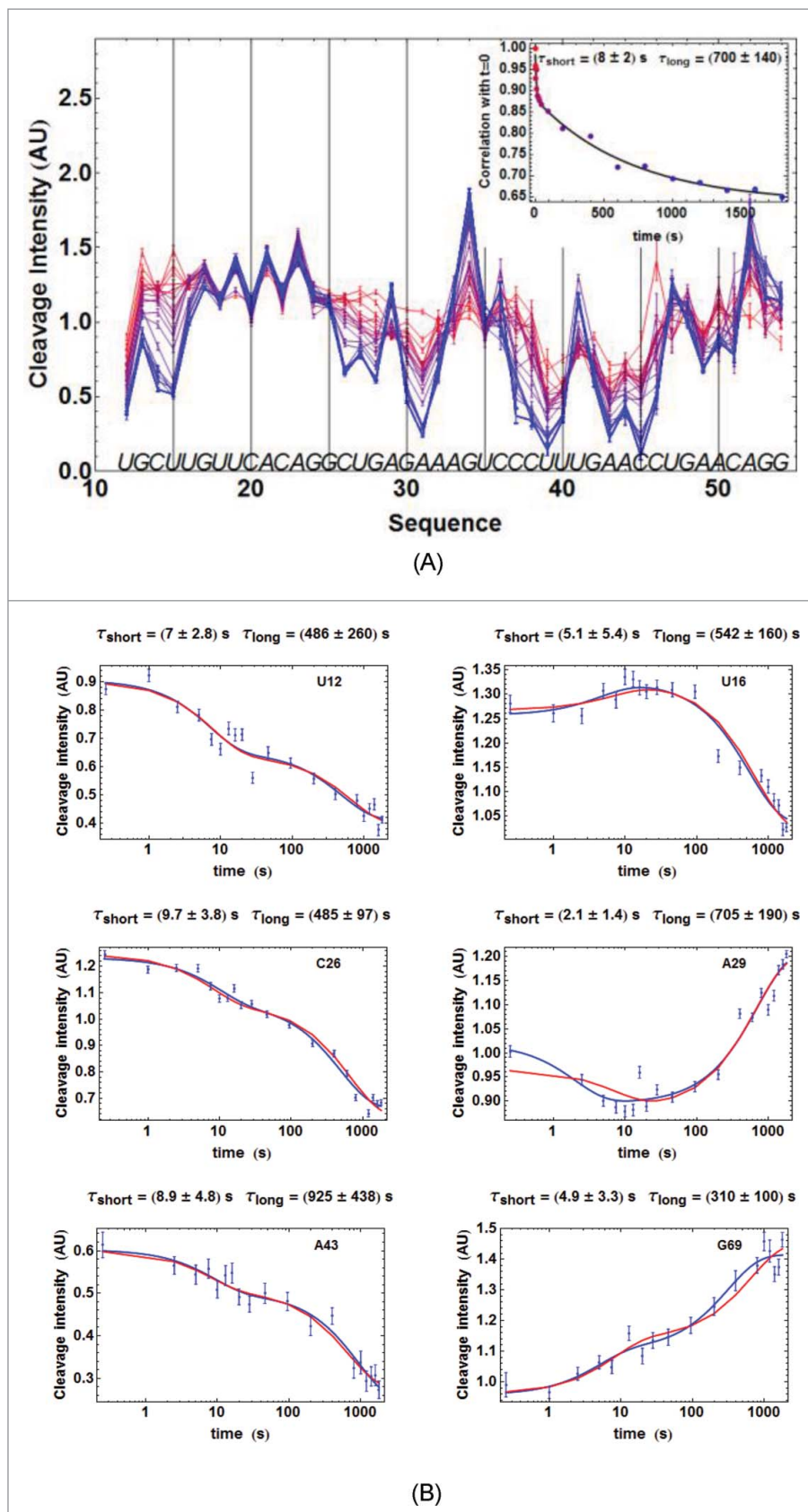
Figure 3. For figure legend, see next page.

Finally, it is of interest of coming back on the large difference in folding kinetics observed for *ATthiC* and *ECthiC*$_{mutP1}$. Such a large difference was surprising for highly similar RNAs. Since it has been reported that a C2′-endo / C3′-endo conformational switch of a single residue could be rate-limiting in RNA folding,[26] we examined whether such a critical residue could explain the slow folding of *ATthiC*. We considered U35 as a candidate because (i) it is both in a C2′-endo and bulged-out conformation in the crystal structure of *ATthiC*, (ii) it has no counterpart neither in *ECthiC* nor in *ECthiC*$_{mutP1}$ and (iii), its counterpart U36 in *ECthiM* is in a different environment as it is flanked on 3′ by a non-canonical A37-G9 base pair, whereas U35 in *ATthiC* is flanked on 5′ by a non-canonical G34-G11 base pair. Surprisingly, ITC showed that a ΔU35 sequence was unable to bind TPP. We can thus only conclude that, in the context of the *ATthiC* sequence, U35 is crucial for shaping a TPP-binding competent riboswitch. Identifying the sequence determinants of *ATthiC* slow folding would deserve a full study.

Disclosing the kinetic mechanism / assessing our methodology

There is now direct evidence from single-molecule fluorescence energy transfer (smFRET) experiments on *ECthiM* [27] that the TPP interacts with a pre-organized riboswitch aptamer following the induced-fit mechanism of kinetic model #1 (equations 1ab). Model #1 was also shown to agree with the results from a single-molecule study of *ATthiC* with optical tweezers.[28] Furthermore, TPP riboswitches are commonly considered as belonging to class II riboswitches (*i.e.*, those achieving complete folding after binding of their ligand).[29] Nevertheless, given the crucial importance of this for the kinetic regulation theory that follows, and also in view of assessing our methodology, we examined this aspect in great details. For that, we performed a comparison of our results obtained with •OH footprinting, *kinITC* and SPR. We also included in the comparison results from a fluorescence study.[23] The rationale is that the correct kinetic model has to be consistent with different techniques monitoring different parameters. We considered in this comparison *ATthiC* (•OH footprinting, SPR), the slightly modified sequence *ECthiC*$_{mutP1}$ for which numerous results were already available (•OH footprinting, *kinITC*, SPR) and *ECthiM* (*kinITC*, fluorescence). A part of the results for *ECthiC*$_{mutP1}$ were presented in [22] to describe the method *kinITC*. Here, the *kinITC* study was extended to *ECthiC* and *ECthiM*.

First, we compared the •OH footprinting results for *ATthiC* showing clear biphasic kinetics (Fig. 3) with SPR results. For that, we attempted to process the SPR experimental curves with both kinetic models. Importantly, it was impossible to fit the experimental curves with model #2, whereas model #1 yielded a good result with the following values for all kinetic parameters (at 25°C): $k_{on} = (3.26 \pm 0.16) \times 10^4$ M^{-1}s^{-1}, $k_{off} = (1.09 \pm 0.02) \times 10^{-3}$s^{-1}, $k_F = (0.39 \pm 0.03) \times 10^{-3}$s^{-1} and $k_U = (1.30 \pm 0.08) \times 10^{-3}$ s^{-1} (thus $k_F + k_U = (1.7 \pm 0.1) \times 10^{-3}$s^{-1}) (Fig. SD-4A). From these values, the corresponding short and long times could be derived from equations 5a,b (Material & Methods) on k_{fast} and k_{slow}, which yielded $\tau_{short} = k_{fast}^{-1} = 15$ s and $\tau_{long} = k_{slow}^{-1} = 595$ s, in reasonable agreement with the fully independent •OH experimental results (Fig. 3A). To go beyond these partial results, we took advantage of the slow folding of *ATthiC* yielding well-resolved •OH cleavage curves (Fig. 3B) to make use of the second processing method with kinetic model #1, which allowed us obtaining k_{on} and $k_F + k_U$ in a way completely independent from SPR (see SD-10 about the fact that only the sum $k_F + k_U$ and not k_F and k_U separately, could be determined). We imposed in this search the value of K_d(overall) obtained independently, which constrained the kinetic parameters of equations (1a,b) to verify $(k_{off} / k_{on})(k_U / k_F) = K_d$(overall). Since K_d(overall) was obtained by SPR and ITC, we used both estimates. The results are in Table 1, which shows that model #1 led to good agreement between the two techniques despite their great difference, and despite the very small number of really free parameters used for extracting kinetic results from the •OH cleavage curves. Particular examples of the joint fit of all cleavage curves are in Fig. 3B.

For *ECthiC*$_{mutP1}$, we compared the SPR and *kinITC* results reported in.[22] However, in[22] the SPR data were processed with a classical single-step mechanism whereas the *kinITC* data were processed with model #1 only. Here, we reprocessed with our own programs all these data with models #1 and #2. At variance with *ATthiC*, the SPR data could be fitted almost equally well with both models (Fig. SD-4BC). However, only model #1 yielded very good agreement with the *kinITC* results for the values of k_{off}, k_F and k_U (Table 2). Both kinetic models led to the same disagreement on k_{on} (see legend of Table 2).

In this work we also submitted *ECthiC* and *ECthiM* to *kinITC* with the experimental protocol described in [22] for *ECthiC*$_{mutP1}$. The fit of all injection curves with model #1 is shown in Fig. SD-5AD, all numerical results are in SD-6AB, the evolution with the temperature of all thermodynamic and kinetic parameters are reported in Fig. 4 for *ECthiM* and in

Figure 3. (figure previous page) Kinetics of *ATthiC* cleavage from •OH footprinting. (A) Each color corresponds to a particular time after TPP addition from $t = 0$ (pure red), to $t = 30$ min (pure blue). The times were 0, 1, 2.5, 5, 7.5, 10, 13, 16, 20, 28, 46, 95, 200, 400, 800, 1000, 1200, 1400, 1600 and 1800 s. Conditions: TPP 2 μM, magnesium acetate 2 mM, sodium cacodylate buffer 5 mM, pH 6.5, 25 °C. The fact that no cleavage variation was observed from G17 to G24, which was not imposed in the processing, is a good indication of the quality of the overall quantification procedure since these residues form a quickly folded apical loop not susceptible to be influenced by TPP binding. Cleavage curves for selected residues are shown in Fig. 3B. A typical gel is shown in Fig. SD-3D. The inset shows the correlation of each cleavage curve with the cleavage curve for $t = 0$ as a function of time, which highlights the biphasic character of the kinetics. (For this correlation curve, the experimental data in the main figure, limited to the residue range U12-G54, were supplemented with other data to cover the wider residue range U12-G69).The solid curve is from a bi-exponential fit; the resulting times τ_{short} and τ_{long} from the fit correspond well with those obtained for individual cleavage curves in Fig. 3B. (B) Kinetics of •OH cleavage for selected residues of *ATthiC*. The experimental points are those for six particular residues (U12, U16, C26, A29, A43 and G69) from Fig. 3A and from other data (not shown). A few experimental points were flagged as outliers and suppressed (*e.g.*, $t = 1$ s for A29 and A43). The two kinds of fit mentioned in the text are shown: in blue, the simple bi-exponential fit (equation 4) and, in red, the fit making use of kinetic model #1 proved to be the correct one in the following (see Fig. SD-10 for an assessment of the quality of fit). The times τ_{short} and τ_{long} reported for each residue result from the bi-exponential fit and are related to k_{fast} and k_{slow} in equation (4) by $k_{fast} = 1 / \tau_{short}$ and $k_{slow} = 1 / \tau_{long}$.

Table 1. Comparison of SPR and $^\bullet$OH results on *ATthiC* for model #1. The indicated values of K_d(overall) (from SPR or ITC) were used to constrain the search of the kinetic parameters with the $^\bullet$OH cleavage curves (see text). The value for K_d(overall)ITC $= 0.35$ μM is the value estimated at 25°C for the major RNA species representing *ca.* 95 % of the active RNA: Fig. SD-17A,C.

	$k_{on}(\mathrm{M}^{-1}\,\mathrm{s}^{-1})$	$k_F + k_U\,(\mathrm{s}^{-1})$
SPR	$(3.26 \pm 0.16)\times 10^4$	$(1.7 \pm 0.1)\times 10^{-3}$
$^\bullet$OH with K_d(overall)SPR $= 0.1$ μM	$(3.5 \pm 2)\times 10^4$	$(2.6 \pm 0.6)\times 10^{-3}$
$^\bullet$OH with K_d(overall)ITC $= 0.35$ μM	$(1.7 \pm 0.9)\times 10^4$	$(3.9 \pm 1.1)\times 10^{-3}$

Fig. SD-7 for *ECthiC*. We could compare our new results on *ECthiM* with those from an independent fluorescence study that was performed by considering 2-aminopurine (2AP) substitution for adenine at seven positions in the aptamer.[23] This allowed Lang *et al.* to obtain, for each modified position, the slow component of the kinetics of 2AP disturbance (at 25°C) upon TPP addition at various concentrations (their Table 1). These raw experimental results yielded a set of seven k_{obs} values with a mean value $<k_{obs}> = 8.7\times 10^4$ $\mathrm{M}^{-1}\mathrm{s}^{-1}$ and a standard deviation of 4.4×10^4 $\mathrm{M}^{-1}\mathrm{s}^{-1}$. From the analysis exposed in SD-9, $<k_{obs}>$ should be comparable to k_{on} for model #1 (equation S9.1), whereas it should be comparable to $k_{on}k_F/(k_F + k_U)$ for model #2 (equation S9.2). The results at 25°C of the *kinITC* experiments yielded $k_{on} = (6.4 \pm 2) \times 10^4$ $\mathrm{M}^{-1}\mathrm{s}^{-1}$ with model 1 and $k_{on}k_F/(k_F + k_U) \approx 2.8 \times 10^4$ $\mathrm{M}^{-1}\mathrm{s}^{-1}$ with model 2 (the error was not estimated). By comparison to $<k_{obs}> = 8.7\times 10^4$ $\mathrm{M}^{-1}\mathrm{s}^{-1}$, model #1 is again favored. We have no independent experiments to be compared with those for *ECthiC*.

In conclusion, all our experimental results on *ECthiC$_{mutP1}$*, *ECthiM* and *ATthiC*, as well as the fluorescence[23] and smFRET[27] experiments on *ECthiM*, and the optical-tweezer experiments on *ATthiC*,[28] are unambiguously in favor of kinetic model #1, which is thus the assumed model in the following.

kinITC results shed light on the kinetic regulation by E.coli riboswitches

The kinetic mechanism being now firmly established we can discuss the results obtained from *kinITC* with model #1. As a consequence of the ability of *kinITC* to dissect the overall process into its two components, TPP binding and RNA folding, the global enthalpic term measured by ITC could be split into

$\Delta H_{\mathrm{Binding}}$ and $\Delta H_{\mathrm{Folding}}$. It appears that $|\Delta H_{\mathrm{Binding}}|$ for *ECthiM* never becomes large (it has a null value at 32°C), whereas $\Delta H_{\mathrm{Folding}}$ becomes more and more negative as the temperature increases (Fig. 4A). Globally, the same features were also observed for *ECthiC* in this work (Fig. 5A) and for *ECthiC$_{mutP1}$*in,[22] which adds support to these observations.

First, that $\Delta H_{\mathrm{Folding}}$ becomes more negative when the temperature increases is consistent with the fact that, upon TPP-triggered folding (implying stabilization), the RNA releases most of the heat stored as thermal agitation during its progressive destabilization in absence of TPP. Second, as a consequence of the van 't Hoff equation linking the ΔH and the K_d of an equilibrium $(\partial lnK_d/\partial(1/T) = \Delta H/\mathrm{R}$, with R the gas constant), a null value of ΔH at some temperature implies that the corresponding K_d is extremum at that temperature and, in turn, varies little around that temperature. This feature is clearly visible for *ECthiC* and *ECthiM* (Fig. 5B) as previously noticed for *ECthiC$_{mutP1}$*.[22] This fact has implications of strong significance because the K_d for the initial step appears to be tuned for the TPP concentration to be regulated ($K_d = 0.9$ μM for *ECthiC* and 0.45 μM for *ECthiM* at 30°C, see tables SD-6AB). On the contrary, K_d(overall) $= K_d / K_F$ is not only strongly variable with the temperature, but is also much too low at all temperatures (less, or much less than 0.2 μM for *ECthiC* (Fig. SD-7A), and less than 0.06 μM for *ECthiM* (Fig. 4A) to be at the basis of a classical thermodynamic regulation. Therefore, these two riboswitches ensure a regulation of kinetic nature and their ability to detect a low TPP concentration appears to be correlated to the K_d for the initial step, not to K_d(overall).

Primary and secondary (late) sites of TPP interaction

Beyond yielding classical kinetic information (through the parameters k_{on} and $k_F + k_U$), the second processing method of $^\bullet$OH footprinting results (see Material and Methods and SD-10) makes use of the firmly established kinetic model, which eventually yields three coefficients $\alpha_0^n, \alpha_1^n, \alpha_2^n$ for each residue. These coefficients represent the propensity of the nth residue to be cleaved in, respectively, the species R_0, R_1, R_2 (equations 1a,b). If a particular residue is sensing early TPP binding, its cleavage propensity is expected to change between the initial state R_0 and the intermediate state R_1. This implies that $(\alpha_1^n - \alpha_0^n)$ should be significantly different from 0. We

Table 2. Confrontation of the two models with SPR and *kinITC* results on *ECthiC$_{mutP1}$*. The values from SPR were obtained at 25°C, and those from *kinITC* were calculated for 25°C from the results obtained at 20, 27, 30, 34 and 37°C. Only model #1 led to excellent agreement for k_{off}, k_F and k_U from the two techniques, whereas model 2 led to serious disagreement for k_F and considerable disagreement for k_U. As already mentioned in [22] for model #1, both kinetic models and both techniques disagree on k_{on} by a factor of 6. However, only *kinITC* is in agreement with the very well determined value of K_d(overall) obtained by ITC after independent measurements at five temperatures.

Model #1	$k_{on}(\mathrm{M}^{-1}\,\mathrm{s}^{-1})$	$k_{off}\,(\mathrm{s}^{-1})$	$k_F\,(\mathrm{s}^{-1})$	$k_U\,(\mathrm{s}^{-1})$
SPR	$(1.28 \pm 0.03)\times 10^5$	0.16 ± 0.025	1.8 ± 0.26	$(3 \pm 0.5)\times 10^{-3}$
kinITC	$(0.26 \pm 0.02)\times 10^5$	0.09 ± 0.006	1.1 ± 0.1	$(3.7 \pm 0.5)\times 10^{-3}$
Model #2	$k_{on}(\mathrm{M}^{-1}\,\mathrm{s}^{-1})$	$k_{off}\,(\mathrm{s}^{-1})$	$k_F\,(\mathrm{s}^{-1})$	$k_U\,(\mathrm{s}^{-1})$
SPR	$(1.39 \pm 0.03)\times 10^5$	$(2.4 \pm 0.1)\times 10^{-4}$	1.5 ± 0.35	$(2.9 \pm 0.7)\times 10^{-2}$
kinITC	$(9.4 \pm 4.4)\times 10^5$	$(3 \pm 1.6)\times 10^{-4}$	0.32 ± 0.08	17 ± 3

(A)

(B)
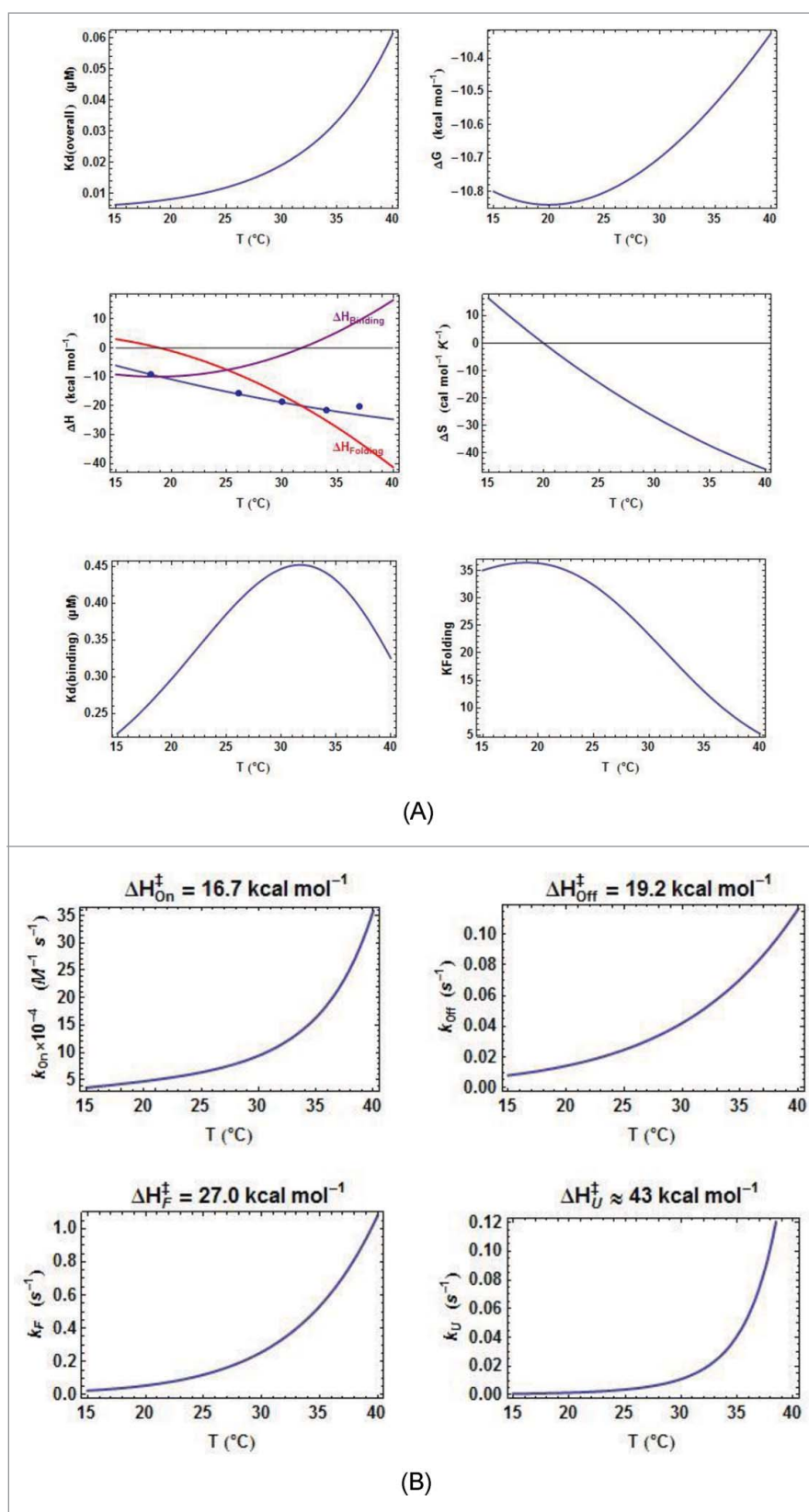
Figure 4. Thermodynamic and kinetic results from *kinITC* for *ECthiM*. (A) Thermodynamic results. The evolution with the temperature of the thermodynamic parameters of all steps in equations 1a,b was obtained with *kinITC* used with model #1. The figures for ΔG and ΔS refer to the complete reaction involving TPP binding and RNA folding. The figure for ΔH collects $\Delta H_{Binding}$, $\Delta H_{Folding}$ (dashed curve) and $\Delta H_{ITC} = \Delta H_{Binding} + \Delta H_{Folding}$ shown in blue with the individual values obtained by normal use of ITC at five different temperatures (blue dots). Note the extremum of K_d reached at the temperature where $\Delta H_{Binding} = 0$ in agreement with the Van't Hoff equation linking K_d(binding) and $\Delta H_{Binding}$. This extremum is here a maximum because $\Delta C_P(Binding) = \partial \Delta H_{Binding}/\partial T$ is positive. The injection curves of the *kinITC* experiments at different temperatures and their fit are shown in Fig. SD-5C. (B) Kinetic results. The evolution with the temperature of all kinetic parameters in equations 1a,b was obtained with *kinITC* used with model #1. The activation energies and $\Delta H_{on}^{\ddagger}$ and $\Delta H_{U}^{\ddagger}$ were obtained as adjustable parameters in *kinITC*, and $\Delta H_{on}^{\ddagger}$ and $\Delta H_{U}^{\ddagger}$ were deduced from $\Delta H_{Binding}^{0} = \Delta H_{on}^{\ddagger} - \Delta H_{off}^{\ddagger}$ and $\Delta H_{Folding}^{0} = \Delta H_{F}^{\ddagger} - \Delta H_{U}^{\ddagger}$, respectively.
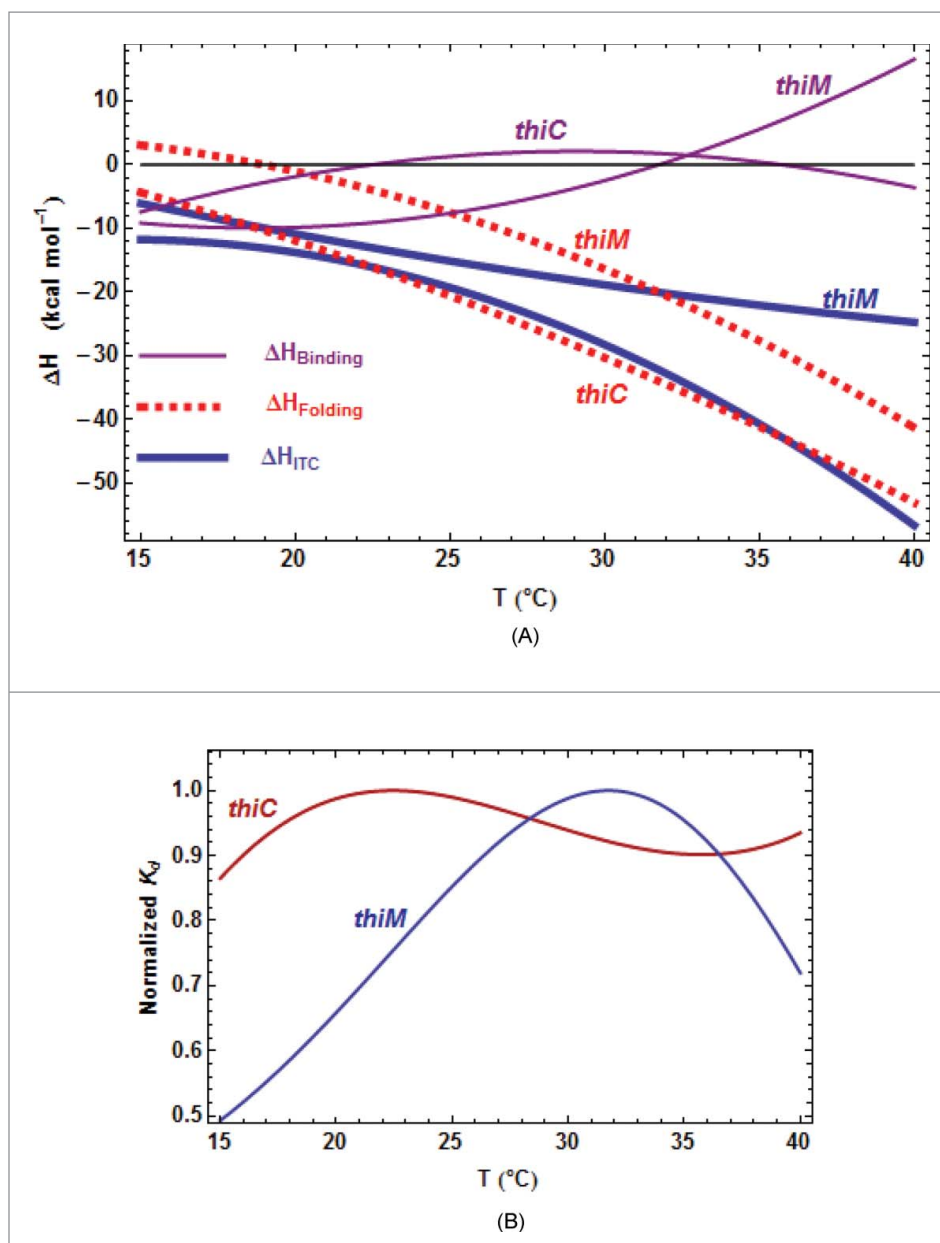
Figure 5. Comparison of the thermodynamic parameters for *E. coli* riboswitches. A. Comparison of all ΔH terms from *kinITC*. The three curves are related by $\Delta H_{ITC} = \Delta H_{Binding} + \Delta H_{Folding}$. The pattern is similar for the two *E. coli* riboswitches: the two $\Delta H_{Binding}$ curves cross $\Delta H_{Binding} = 0$ at nearby temperatures and the two $\Delta H_{Folding}$ curves are quasi parallel. B. Quasi absence of temperature variation for K_d. Each K_d curve has been normalized to a unit value at its maximum (0.93 μM for *ECthiC* and 0.45 μM for *ECthiM*). K_d is almost constant for *ECthiC* and varies at most twofold for *ECthiM* in a broad temperature range in comparison of K_d (overall) which varies tenfold for *ECthiM* (Fig. 4A) and more than thirtyfold for *ECthiC* (Fig. SD-7A).

have represented the evolution along the sequence of this difference normalized by its e.s.d, *viz.* $(\alpha_1^n - \alpha_0^n) / \sigma(\alpha_1^n - \alpha_0^n)$, which shows remarkably well that the primary binding of TPP occurs *via* its pyrimidine ring into the conserved loop sequence **UGAGA** between P2 and P3 (Fig. 2D, Fig. 6AB). This is particularly clear for *ATthiC*, which does not show any primary binding in the P4/P5 junction where the pyrophosphate moiety eventually interacts, whereas *EcthiC_mutP1* shows slight primary binding in the P4/P5 junction (Fig. SD-11A). These results fit well with those obtained by chemical probing in[30] and with a study that showed that thiamine (corresponding to TPP deprived of pyrophosphate) can bind like TPP within the pyrimidine binding pocket without any contact with the (disordered) pyrophosphate-binding pocket.[31] Analogous

conclusions derive from crystal structures of *ECthiM* bound to TPP, TMP and pyrithiamine also deprived of pyrophosphate.[32] Therefore, this confirms that prior pyrophosphate binding is not necessary for pyrimidine binding and this also shows (at least for *ECthiM* studied in[31,32]) that the pyrophosphate-binding pocket becomes ordered only upon interaction with the pyrophosphate. Also adding support to our results is the K_d value of 1.5 μM reported for thiamine/*ECthiM* interaction,[33] which is close to $K_d = 0.45$ μM obtained with *kinITC* (SD-6B) for the initial binding step of TPP comparable to thiamine binding.

The same analysis performed with $(\alpha_2^n - \alpha_1^n) / \sigma(\alpha_2^n - \alpha_1^n)$ highlighted the secondary (or late) TPP interaction occurring during the second kinetic step (Fig. SD-
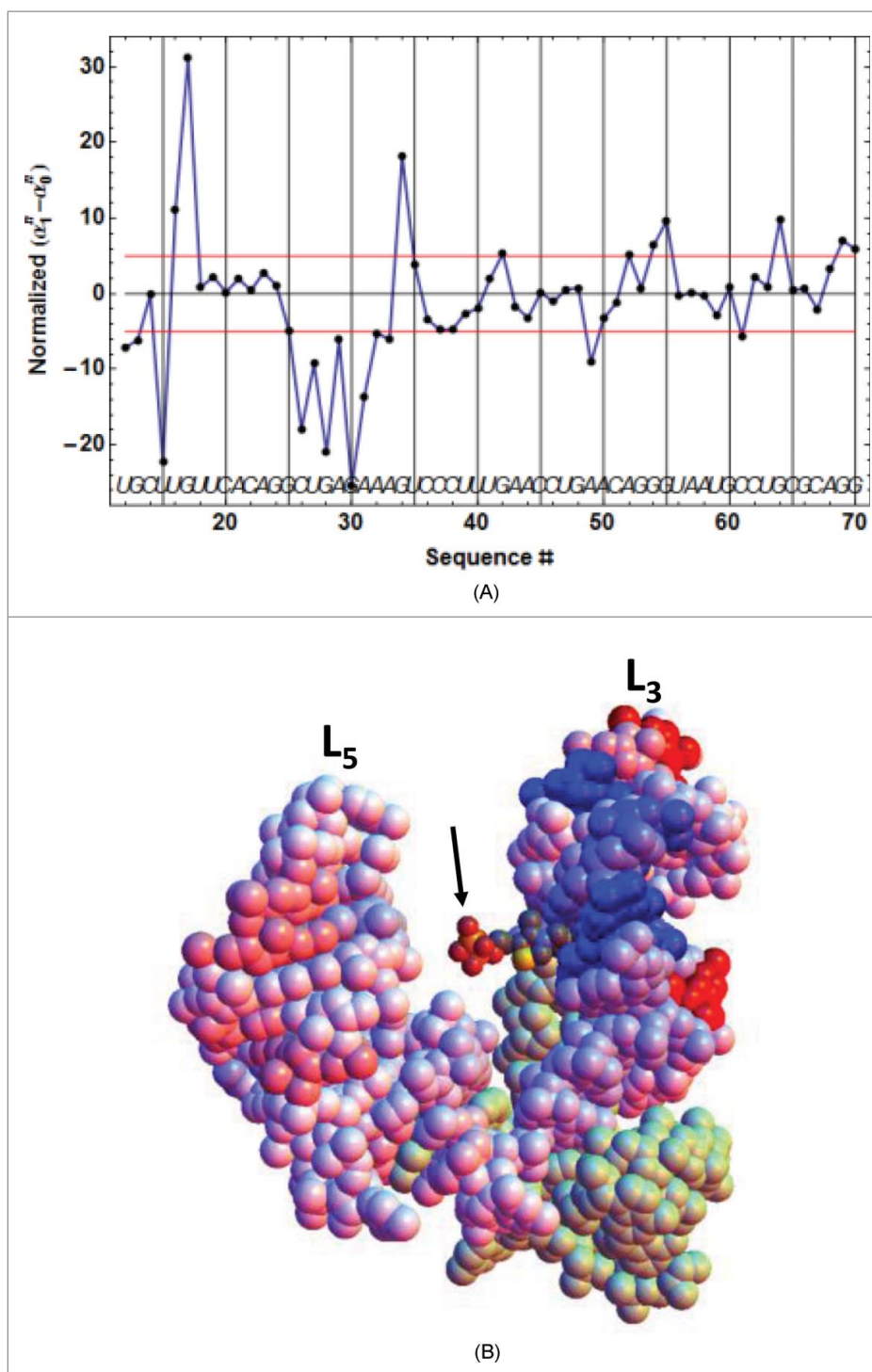
Figure 6. Primary TPP/RNA interaction for *ATthiC*. (A) The evolution along the sequence of the normalized difference $\left(\alpha_1^n - \alpha_0^n\right) / \sigma\left(\alpha_1^n - \alpha_0^n\right)$ (see text) is shown. A large negative (resp. positive) value of the difference is the mark of early protection against cleavage (resp early enhanced cleavage) after TPP addition. The red lines mark the positive and negative limits at a 5σ threshold. B. The closed riboswitch from the crystal structure has been opened to visualize the primary interaction of the TPP with the RNA; only the pyrophosphate of the TPP is visible (arrow). The loops L5 and L3 are labeled (Fig. 2D). The colors evolve from pure blue to pure red for, respectively, the most negative and most positive values of the normalized difference $\left(\alpha_1^n - \alpha_0^n\right) / \sigma\left(\alpha_1^n - \alpha_0^n\right)$ shown in Fig. 6A. The greenish color corresponds to the 5'-end and 3'-end residues for which no accurate results were obtained. All significantly negative values (pure blue), as well as the highest positive values (pure red), are exclusively located around the interaction site of the TPP pyrimidine moiety.

11BC). Particularly striking is the protection of C14 and C26 in P3 by the closing of the apical loop L5, and the protection of G60 by the formation of a close contact with the TPP. Altogether, these results are perfectly consistent with kinetic model #1.

Determination of ON/OFF-state probabilities for kinetically-regulated riboswitches

As a major consequence of the previous results, we developed a quantitative model of kinetic regulation. For that,
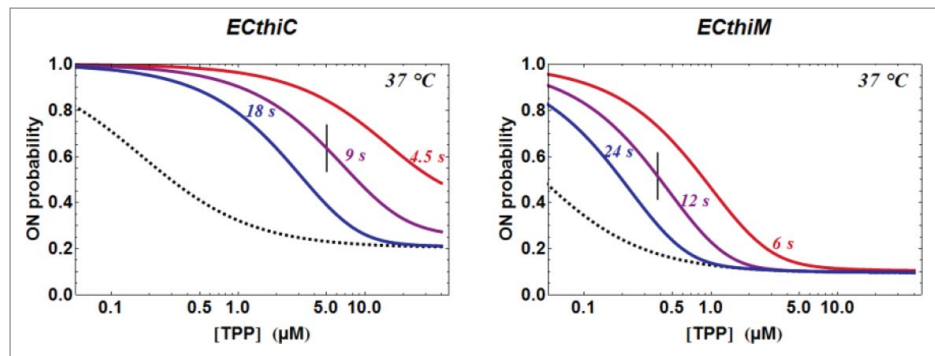
Figure 7. TPP concentration dependence of the kinetic regulation by *ECthiC* and *ECthiM*. The dependence of P_{ON} on the TPP concentration from equation (3) is shown (solid curves) for a common temperature (37°C) and for three values of t_S. The value for each middle curve (9 s for *ECthiC* and 12 s for *ECthiM*) corresponds to the experimental pausing time observed at 37°C with NusA. The vertical bar on each middle curve marks the inflection point where the regulation efficiency is maximum. The two other curves corresponding to half and twice the pausing time are shown to illustrate the effect of this parameter on the regulation. The black dashed curves correspond to P_{ON} that would be obtained if each riboswitch was thermodynamically, and not kinetically controlled, which emphasizes the strong kinetic character of the regulation.

we sought to express, as a function of the ligand concentration and of all relevant kinetic parameters, the probabilities P_{ON} and $P_{OFF} = 1 - P_{ON}$ for a kinetically-regulated riboswitch to be in the ON- and OFF-state, respectively. These considerations extend those in [17] where the binding of the ligand

to an adenine riboswitch was modeled satisfactorily with one kinetic step. Here, we take in consideration the two-step mechanism of model #1. Negative regulation (corresponding to the OFF-state) results from the formation of the species R_2 (equation 1b) due to stable binding of TPP to the newly
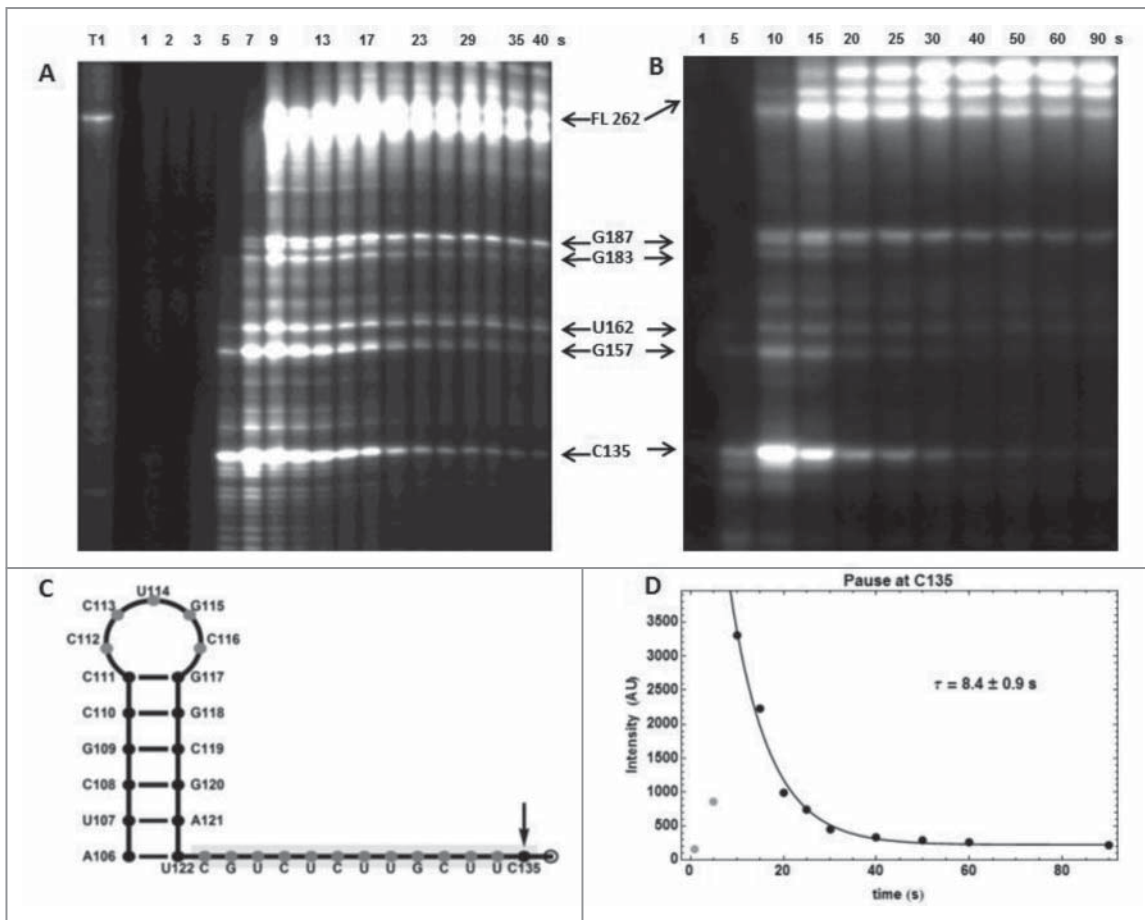
Figure 8. RNA polymerase pause sites observed during *ECthiC* template transcription. (A) Transcription kinetics without nusA (see SD-15AB). Transcription times are indicated on top of the gel. Pause sites positions are indicated on the right (FL: full length transcript). The leftmost lane is an RNAse-T1 ladder. Significant pausing is visible at upstream positions of C135. Transcription was performed at 30°C. (B) Transcription kinetics with NusA (0.3 μM). Pausing at C135 is now prominent as compared to A. Transcription experiment was performed at 37°C. (C) Sequence upstream of the pausing site at C135. The footprint of the polymerase is indicated by the gray rectangle. The hairpin structure forms a class I pause site according to.[39] (D) Kinetic analysis of pausing at C135. The exponential time $\tau = 8.4$ s corresponds to the average pausing time. The points corresponding to 1 and 5 s (in gray) were not used in the fit.

synthesized aptamer, importantly before the polymerase has reached a point where it cannot be halted anymore for transcription regulation, or within the time left for the ribosome to bind to the Shine-Dalgarno sequence for translation regulation. If we note t_S (noted Δt_{RNAP} in [17]) the average time necessary for the polymerase to reach such a critical switching point, the probability P_{OFF} is thus equal to the probability of formation of the species R_2 after t_S. This probability is nothing else than the molar fraction of R_2 formed at $t = t_S$ with $R_1 = R_2 = 0$ at $t = 0$. From equation (4) in Materials and Methods, it is thus obtained:

$$P_{ON} = 1 - \tilde{R}_2 - f_2 exp(-k_{fast}t_S) - s_2 exp(-k_{slow}t_S) \quad (3)$$

with $\tilde{R}_2 = K_F(1 + K_F + K_d/L_{tot})^{-1}$ being the fraction of R_2 at equilibrium (equation S8.3c in SD-8), k_{slow} and k_{fast} being given by equation (5a) and the coefficients f_2 and s_2 by equations S8.5. The dependence of P_{ON} on the logarithm of L_{tot} shows the characteristic sigmoid shape of a 'logistic function' (Fig. 7). However, equation (3) is not a 'general-purpose' equation involving adjustable parameters; instead it makes an explicit link to, and only to, the ligand concentration L_{tot} and the measurable kinetic parameters $t_S, k_{on}, k_{off}, k_F, k_U$ (since all parameters $\tilde{R}_2, f_2, s_2, k_{fast}$ and k_{slow} in equation (3) can be calculated from $k_{on}, k_{off}, k_F, k_U$ and L_{tot}). One may thus expect legitimately that the position of the inflection point of the sigmoid curve, which only depends on these measurable parameters, should correspond to the expected TPP concentration of the ON/OFF switching point. We will see that this is indeed the case.

From equation (3), it is clear that an increase of t_S would shift progressively the regulation from a dominant kinetic regime to a purely thermodynamic regime corresponding to $P_{ON} = 1 - \tilde{R}_2$, which is illustrated in Fig. 7 with three values of t_S. The kinetic parameters $k_{on}, k_{off}, k_F, k_U$ being determined (at a given temperature) for a particular riboswitch, only t_S can thus influence the ligand concentration of the ON/OFF switch. As we have seen (introduction), this switch has to occur when the TPP concentration lies broadly in the micromolar range, which is precisely the order of magnitude of the K_d values of the initial step obtained by *kinITC*. Interestingly, equation (3) gives deep insight into a condition ensuring that this K_d value would be the TPP concentration around which the ON/OFF switch occurs. (This obviously does not mean that the switch has to occur exactly at the K_d, but that the K_d value defines a range of concentration for the switch). At variance with the usual and practical definition of the ON/OFF switch corresponding to the ligand concentration at half-maximum response, we define it as the inflection point of the sigmoid curves where the variation of ligand concentration has the greatest effect (Fig. 7). We think this is the appropriate definition since it corresponds to an intrinsic property not biased by the responses at high and low ligand concentrations. On a practical ground, however, the two definitions are more or less equivalent. The full mathematical expressions (equations 3 and 5a,b) are too involved to be used directly for the determination of the inflection point. However, as explained in SD-8 (equation S8.5c *et seq.*), the term $f_2 exp(-k_{fast}t_S)$ becomes rapidly

negligible in comparison of $s_2 exp(-k_{slow}t_S)$, which greatly simplifies the problem. An analysis based upon carefully checked approximations (detailed in SD-12) showed that the inflection point of the regulation curve lies at a TPP concentration very close to $(k_{on}t_S)^{-1}$, which corresponds to $K_d = (k_{on}/k_{off})^{-1}$ if t_S is equal to k_{off}^{-1}. This theoretical conclusion was perfectly confirmed by numerical calculations (Fig. SD-12A,C). The major result of this study, therefore, is that the overall time t_S left for ligand binding has to be roughly of the order of k_{off}^{-1} to obtain a regulation in the right range of TPP concentration, which is a strong prediction of our quantitative model. There is an apparent contradiction with one conclusion in [17] stating instead that t_S has to be significantly smaller, or much less, than k_{off}^{-1}. The contradiction disappears when considering the different meaning of k_{off} in [17] and in this work (see SD-13). Before examining the validity of this prediction we consider other consequences of the model.

A kinetic regulation is more efficient than a thermodynamic regulation

A 'kinetic regulation efficiency' (KRE) can be defined by the steepness of the response to concentration variation of the ligand. Such steepness can be quantified by considering the slope $|dP_{ON} / d(log10 L_{tot})|$ at the inflection point (Fig. SD-12C). Interestingly, the exposed model allows estimating this slope (SD-14), which shows that this KRE is very close to $ln(10) e^{-(1+1/K_F)}$ for any riboswitch ensuring a kinetic regulation according to model #1. In addition, if $K_F \gg 1$, the index is close to the universal maximum value $KRE_{max} = ln(10) e^{-1} \approx 0.847$. In general, one thus has $KRE \approx KRE_{max} e^{-1/K_F}$. When $K_F \gg 1$, this implies that a 4-fold increase of the ligand concentration around the switching point makes P_{ON} drop by *ca.* 1/2 (from ~0.65 to ~0.15).

For a classical thermodynamic regulation based upon mass action law, a 'thermodynamic regulation efficiency' (TRE) index can also be estimated from $|dP_{ON} / d(log10 L_{tot})|$ (see SD-14), which also yields a universal value $TRE = ln(10) / 4 \approx 0.576$. This universality is in agreement with the analysis in [34] for thermodynamically regulated riboswitches. (It is interesting to compare our 'ideal' value $TRE \approx 0.576$ with the results obtained in [34] by numerical simulations. From Fig. 2C in,[34] we derived the lower value $TRE \approx 0.45$, which fits with a decrease of efficiency resulting from mRNA degradation taken into account in the simulations). According to our results, a 'kinetic regulation' is thus intrinsically more efficient than a 'thermodynamic regulation' since $KRE_{max} / TRE = 4e^{-1} \approx 1.47$. More precisely, with a 'thermodynamic regulation', a 4-fold increase of the ligand concentration from $L_{tot} \approx K_d / 2$ to $L_{tot} \approx 2K_d$ makes P_{ON} drop by 1/3 only (from 2/3 to 1/3), and not by 1/2 as with a 'kinetic regulation'. To recover the same drop of P_{ON} by 1/2, a thermodynamic regulation requires a 9-fold increase of the ligand concentration from $L_{tot} = K_d / 3$ to $L_{tot} = 3K_d$. In conclusion, a kinetic regulation produces a steeper response than a thermodynamic regulation, which leads to a more accurately defined concentration of the ON/OFF switch. This rationalizes the interest of a kinetic regulation. Noteworthy, analogous conclusions were reached empirically after numerical simulations in.[17]

RNA polymerase pauses and kinetic regulation

The fact that the RNA polymerase pauses at critical locations is at the basis of riboswitch-mediated kinetic regulation.[17,18,35-37] Indeed, a kinetic regulation results from these pauses leaving the appropriate time to the ligand for binding to the riboswitch aptamer, but only when its concentration is high enough. We thus first verified the existence of pauses for the 2 *E. coli* riboswitches (Fig. SD-15B), next we determined the pausing times and, finally, we compared these results with the predictions of our kinetic-regulation model.

For *ECthiC*, we observed a strong pause site at C_{135} downstream of the aptamer domain (Fig. 8A-B). That it can be seen as a programmed pausing site is corroborated by the existence of a stable hairpin-loop (A_{106}-U_{122}) upstream of the pause site (Fig. 8C), thus forming a canonical transcription pausing site.[38] From the exponential decrease of the intensity of the corresponding band on gel we derived an average pausing time of the polymerase at C_{135} of (5.8 ± 0.3) s at 30°C (Fig. 8A) and (5.2 ± 0.4) s at 37°C (not shown). Since the protein NusA is known to increase the pausing time,[39,40] the analysis was repeated with *E. coli* NusA, which yielded the enhanced value (8.4 ± 0.9) s at 37°C (Fig. 8B, D). These pausing times should be increased slightly to take into account the time necessary for the polymerase to reach the pausing site from the end of the aptamer, say *ca.* 2 s (this is not critical). With $k_{on} = (22 \pm 7) \times 10^3$ M^{-1} s^{-1} obtained from *kinITC* at 37°C and from previous theoretical analysis on the determination of ON/OFF-state probabilities, one derives with $t_S \sim 8+2 = 10$ s that the ON/OFF switch takes place around a TPP concentration equal to $(k_{on} t_S)^{-1} = (6.1 \pm 2.4)$ μM without NusA and to $(4.5 \pm 2.)$ μM with NusA. It is interesting to compare the observed pausing time ($\sim 8+2 = 10$ s with NusA) with the theoretical value $k_{off}^{-1} \approx (52 \pm 5)$ s ensuring that the regulation would take place around a TPP concentration equal to the K_d of the initial step (*i.e.* 0.85 μM). The value of the ratio $k_{off}^{-1}/(\text{pausing time}) \approx 5.2$ simply means that the regulation takes place at a concentration roughly 5 times above the K_d.

For *ECthiM*, we observed 2 strong pauses at the close sites C_{153} and G_{159}, and 2 weaker pauses at G_{107} and at G_{128} of the AUG codon (Fig. SD-16). Pausing was already mentioned in the same region of the *ECthiM* expression platform,[41] but we could not make a detailed comparison of our results with those in.[41] With several consecutive pause sites contributing to the overall pausing time t_S, the observed kinetics of pausing at the 3'-pause-site is also affected by the incoming flux of RNA polymerase from the upstream pause-sites. Therefore, the observed pausing time t_S at G_{159}, including the effect of the upstream pausing sites, is the relevant pausing time for the kinetic regulation mechanism. As for *ECthiC*, upon addition of NusA at 37°C, the pausing time increased, but marginally from (8.2 ± 1.9) s to (10 ± 1.2) s. With the value $k_{on} = (22 \pm 6.6) \times 10^4$ M^{-1}s^{-1} obtained with *kinITC* at 37 °C (Fig. 4B) and $t_S \approx 10 + 2 = 12$ s, one derives that the regulation takes place around a TPP concentration equal to $(k_{on} t_S)^{-1} = (0.38 \pm 0.2)$ μM. Finally, we can compare the observed pausing times at 37 °C (~ 12 s) with the theoretical value k_{off}^{-1}. With k_{off} at 37 °C from *kinITC*, it is obtained $k_{off}^{-1} = (11.6 \pm 1)$ s. Here, the agreement with the observed pausing time is excellent,

which means that the regulation takes place around a TPP concentration very close to the K_d of the initial step (*i.e.*, 0.4 μM).

It may thus be emphasized that the kinetic-regulation model, only supplemented with experimental values from *kinITC* (that is without any adjustable parameters), yielded the order of magnitude for the pausing time of the RNA polymerase for *ECthiC*, and an accurate value of it for *ECthiM*. Furthermore, the switching TPP concentration deduced from the model is around 4.5 μM for *ECthiC* and around 0.4 μM for *ECthiM* (at 37°C). Again, there is good agreement between the predictions of the model and the expected range of TPP concentration where the ON/OFF switch has to take place (see Introduction and SD-1).

ATthiC is under thermodynamic control

Although we could not obtain for *ATthiC* the rich amount of information that was obtained with *kinITC* for *ECthiC* and *ECthiM*, we nevertheless obtained with SPR all kinetic parameters at 25°C, which yielded $k_{off} = 1.1 \times 10^{-3}$ s^{-1} and $k_F + k_U = 1.7 \times 10^{-3}$ s^{-1} (Fig. SD-4A). According to the considerations in SD-9, these close values imply that the separation between the linear and saturation regimes for $k_{slow}(L_0)$ is close to $2(k_F + k_U)/k_{on} \approx 0.1$ μM, well below the usual TPP concentration. As a consequence, k_{slow} is almost independent of the TPP concentration since it is close to its asymptotic value $k_F + k_U$ and no kinetic regulation is possible (at least around 25°C). This is in agreement with the fact that $K_d(\text{overall})$ obtained by ITC (Fig. SD-17A) varies from less than 0.3 μM below 20°C to more than 1 μM above 35°C (Fig. SD-17B). Such values of $K_d(\text{overall})$ are much higher than those for *ECthiC* and *ECthiM* and appear to be well tuned for a thermodynamic regulation. Therefore, the regulation by *ATthiC* is under classical thermodynamic control around a TPP concentration equal to $K_d(\text{overall})$. The absence of a kinetic regulation is not surprising for a 3'-UTR riboswitch that neither affects early transcription arrest, nor translation inhibition.[12,42] Admittedly, the latter conclusion is based upon the $K_d(\text{overall})$ values valid for *ca.* 95 % of the RNA population (see SD-17A and SD17C).

ITC experiments in the Single Injection Mode (SIM) allowed us obtaining raw kinetic information at different temperatures for *ATthiC* (Fig. SD-2A). The major result is that the kinetics of complete riboswitch folding/closing is extremely temperature-dependent with an overall activation energy of (44.7 ± 1.7) kcal mol^{-1} at 26 °C and (32 ± 1.7) kcal mol^{-1} at 37 °C (the Arrhenius plot is significantly curved: Fig. SD-2B). As a consequence, the TPP-triggered folding takes 3 min at 37 °C, more than 4 min at 34 °C, and almost 30 min at 26 °C (the latter value being in perfect agreement with •OH results obtained at a much lower TPP concentration: see Fig. 3). An extrapolation from 26 °C making use of the activation energy at 26 °C (a conservative hypothesis) indicates that complete folding would take at least ~ 10 hours at 15 °C and ~ 6 days at 5 °C. Therefore, *ATthiC* appears to be 'frozen' at low temperatures commonly experienced by plants like *A. thaliana*. Altogether, these kinetic considerations suggest that *ATthiC* riboswitch might act as a thermosensor too. Since *ATthiC* regulates

alternative splicing, it is of interest to mention that, *FLM*, a set of transcription factor genes involved in the regulation of flowering in *A. thaliana*, has been shown to be subject to temperature-dependent alternative splicing.[43] This, at least, corroborates the need for such a functionality in *A. thaliana* and supports the suggestion that *ATthiC* might regulate alternative splicing in a temperature-dependent way too.

Discussion

We have clearly established that the 3 TPP riboswitches examined in this work function according to an induced-fit mechanism. However, the regulation by the 2 *E. coli* riboswitches is kinetically controlled, whereas the regulation by *A. thaliana* riboswitch is thermodynamically controlled. We have developed an efficient and predictive model linking all kinetic parameters of the induced-fit mechanism to the kinetic regulation. An interesting result from this model is that any kinetically controlled riboswitch of that kind may ensure its regulation activity around a specific ligand concentration, but always with the same, or almost the same, 'kinetic regulation efficiency'. *ECthiC* and *ECthiM*, for example, regulate the TPP concentration around significantly different values, respectively $\sim$5 μM and $\sim$0.5 μM (at 37 $^\circ$C), but equal relative variations of the concentration around each specific value would induce almost the same effect on the regulation. This means that *ECthiC* appears to be specialized for a TPP high-concentration range 1.5-15 μM, and *ECthiM* for a low-concentration range 0.2-1.5 μM. Such results are of interest for the understanding of a complex regulation network with several riboswitches (as this is the case for the TPP regulation network in *E. coli*[3]). In particular, the tuning of each riboswitch to a specific concentration range of the ligand is likely related to its position within the TPP biosynthetic network. Examination of Fig. 1 shows that the production of HMP-PP by thiD (*thiM* operon) is an obligatory step that can only occur **after** all steps depending on the *thiC* operon. One may thus speculate that, when the TPP concentration is decreasing, the OFF-to-ON switch of *ECthiC* occurs likely before that of *ECthiM, i.e.* at a higher TPP concentration. We note that this is in agreement with our results ($\sim$4.5 μM for *ECthiC* vs. $\sim$0.5 μM for *ECthiM*). Interestingly, such a variability of the ON/OFF switch ligand concentration is well documented for S-adenosyL-methionine (SAM) riboswitches for which the SAM concentration at half-maximum response was found to vary from 0.35 μM to 4 μM for 8 related riboswiches, with 2 'outliers' responding around 15 and 40 μM.[44]

Kinetic regulation by riboswitches is based on a well-defined lapse of time t_S left for ligand binding to the riboswitch aptamer. This can be decomposed into $t_S = t_{pol} + t_{pause}$ with t_{pol} the time necessary to polymerize at normal speed the intervening sequence from the end of the aptamer up to the decision point, and t_{pause} the RNA-polymerase pausing time at specific loci. For *ECthiC* and *ECthiM*, as well as for the cases reported in [17,18,35-37], t_{pause} makes the major contribution to t_S. We arrived for example at $t_{pol} \approx 2$ s and $t_{pause} \approx 8$ s for *ECthiC*, and $t_{pol} \approx 2$ s and $t_{pause} \approx 10$ s for *ECthiM*. However, there is *a priori* no reason as to why $t_S = t_{pause} + t_{pol}$ could not be obtained with $t_{pol} > t_{pause}$, and even with

$t_{pause} = 0$. Since $(k_{on}t_S)^{-1}$ determines the ligand concentration L_S of the ON/OFF switch (hence $t_S = (k_{on}L_S)^{-1}$), a likely limitation of a putative pause-free kinetic regulation is on the upper limit of $t_S = (k_{on}L_S)^{-1}$ for not having to synthesize an unreasonably long intervening sequence to achieve regulation. For example, on the basis of a transcription rate of $\sim$50 nt s^{-1}, it would be necessary to synthesize as much as 450-500 nt for *ECthiC* and 550-600 nt for *ECthiM* to reproduce the values of t_S observed with pausing, respectively 10 and 12 s. However, it would suffice that k_{on} and L_S be each greater merely by a factor of 2 to lower $t_S = t_{pol}$, and hence the length to be transcribed, by a factor of 4. One may thus envision the possibility of a kinetic regulation without significant pause(s) of the RNA polymerase.

The variability of the important parameter t_S is a versatile way of dictating the ligand concentration of the ON/OFF switch. It can manifest itself among different riboswitches because of the variability of their sequence to be transcribed or, for a given riboswitch, because of the variability of the expression, or availability, of factors like NusA and NusG.[45] Of course, a significant stochastic variability of t_S is also to be expected, which would be particularly significant for low-copy number mRNAs. We think that further analysis on these different topics will require studying the collective behavior of the full TPP biosynthetic network comprising several genes being controlled by TPP riboswitches.[3] In particular, to be realistic, such network simulations require taking into account other parameters than those bearing merely on riboswitch functioning, *e.g.* mRNA and protein degradation, as performed in.[34] We have taken steps toward that goal. We note that our model of kinetic regulation by *ECthiC* and *ECthiM* cannot be compared to the numerical simulations in[34] that were based on model #2 (conformational change before ligand binding), whereas our experimental results implied to use model #1.

Finally, it is of interest of addressing the important question of new antibiotics development. Indeed, finding TPP analogs that, on one hand, could turn off the expression of genes involved in the biosynthesis of TPP but that, on the other hand, could not be used as cofactors of crucial enzymes would be a valuable route to fight pathogenic bacteria.[46-49] The success of such a strategy depends on the ability of such analogs to lure the regulation mechanism to the point that gene expression is switched off even though the TPP concentration is becoming too low. Our results on kinetic regulation imply that the in-cell concentration L_A of the TPP analog has to be of the order of, or above $(k_{on}t_S)^{-1}$ or, put differently, $k_{on}L_A > t_s^{-1}$. This means roughly $k_{on}L_A > 0.1$ s^{-1} at 37 $^\circ$C for *ECthiC* and *ECthiM* if one considers the approximate value $t_S \approx 10$ s for both. Since kinetic parameters are involved, one should keep in mind the possibility of a significant influence of the temperature on this criterion. Of course, these considerations on TPP riboswitches can be extended to all other kinetically-regulated riboswitches. They indicate how the relevant parameters k_{on}, L_A and t_S provide us, at least in theory, with an objective criterion for a successful hijacking of kinetic regulation for therapeutic purpose. In practice, this obviously cannot replace the assessment of candidate molecules by monitoring directly the expression of the targeted genes, as mentioned in.[48]

Materials and methods

RNA preparation

The aptamer domains of *ECthiC* and *ECthiM* genes were cloned in pRZ plasmid [50] under the control of the T7 RNA polymerase promoter. For *ECthiC*, a mutated form in helix P1 (noted *ECthiC$_{mutP1}$*), prepared initially for crystallization experiments, had already been used for $^{\bullet}$OH footprinting experiments, as well as for *kinITC* and SPR experiments.[22] Here, we prepared the *wt* sequence (*ECthiC*) for new *kinITC* experiments. The aptamer domain of *ATthiC* was cloned in pUC19 plasmid.[51] Linearized plasmids were used for *in vitro* run-off transcription by T7 RNA polymerase according to usual protocols. The RNA products were further purified on DNA Pac100 column (Dionex, Thermo Fischer Science) and relevant fractions were extensively washed with water and concentrated on Centricon 10K (Millipore). For $^{\bullet}$OH footprinting experiments, RNA was 5′dephosphorylated using Fast AP enzyme from Fermentas (Thermo Fischer Scientific), then ^{32}P 5′-radiolabelled when required, according to usual protocols using Polynucleotide kinase (New England Biolabs) and ATP-γ^{32}P (Hartmann, Germany). The labeled RNA was gel purified, eluted, precipitated and resuspended in water.

RNA solutions in water, at 60 nM and 60 μM for footprinting and ITC experiments respectively, were heated at 90°C for 4 min and let stand for 40 min at room temperature. Ten-fold concentrated buffer (sodium cacodylate pH 6.5, 0.5 M; potassium acetate 1 M; magnesium acetate 50 mM) was then added and the mixture was incubated for 40 min at room temperature.

Hydroxyl-radical footprinting experiments

We used a Kintek RQF-3 quench flow apparatus with the protocol described in.[52] Final concentrations are indicated in the following. Briefly, the renatured RNA (30 nM) was rapidly mixed with a solution containing TPP (from 2 to 60 μM) and 0.3 % H_2O_2 (Sigma). The RNA/TPP mixture was incubated for various times (from 15 ms to *ca.* 100 s for *ECthiC$_{mutP1}$*, but from 15 ms to 1800 s for *ATthiC*) before addition of Fe-EDTA (6 mM-6.6 mM) to generate hydroxyl radicals ($^{\bullet}$OH). The probing reaction (in 30 μl) was rapidly quenched after 15 ms with 600 μl of ethanol and the RNA was resuspended in gel-loading solution. The cleavage products were resolved on 10% polyacrylamide gels in denaturing conditions. Gels were dried, exposed on imaging plates and scanned on a Bioimage Analyzer (Fuji Photo Film Co, Ltd).

ITC experiments

Experiments were performed at various temperatures on an ITC$_{200}$ apparatus (Microcal, GE-Healhtcare Northampton MA, USA). Renatured RNA was loaded in the cell (from 20 to 60 μM) and the TPP in the syringe (buffer used: sodium cacodylate pH 6.5, 50 mM; potassium acetate 100 mM; magnesium acetate 5 mM). To obtain thermodynamic information ITC was used in the classical multiple-injection mode. Experimental data processing was performed with our own methods and programs. We have taken steps for their introduction into the program *AFFINImeter* (S4SD,

Santiago de Compostela, Spain). We also made use of *kinITC* [22] to obtain complete kinetic information (see below). Raw kinetic information was also obtained for *ATthiC* through experiments in the single-injection mode (at different temperatures).

SPR experiments

SPR experiments with *ATthiC* were performed on a Biacore 2000 instrument using Research Grade CM5 sensor chips (GE Healthcare). RNA constructs were prepared and experiments conditions were conducted as described for *ECthiC$_{mutP1}$* in[22] (same buffer as for the ITC experiments). Experimental data were acquired in single-cycle mode[53] and processed with our own program, either with the 2-step 'induced-fit' model #1, or conformational selection model #2. The equations necessary for this processing are described in the following. The theoretical SPR signal in Resonance Units (RU) was considered to be proportional to $R_1(t) + R_2(t)$ for model #1, and to $R_2(t)$ for model #2 (equations 1a-b, 2b). The kinetic parameters were derived from a joint fit of 2 experimental data sets.

In vitro transcription by E. coli RNA-polymerase

DNA templates were first synthesized by PCR. Under the control of the T7A1 promoter, the sequences contain the full length riboswitch (*ECthiC* or *ECthiM*) and the first 60 nucleotides of the downstream gene (*thiC* or *thiM*) (SD-15A). *In vitro* single-round transcription experiments were performed at 37°C in buffer (30 μl) containing 40 mM Tris HCl (pH 7.5), 150 mM KCl, 10 mM MgCl2, 0.01 % Triton X-100. DNA templates (100 nM final concentration) were first incubated for 10 min with *E. coli* RNA polymerase (Epicentre) (100 nM final concentration), GTP, ATP, UTP (25 μM final concentration) and [α^{32}P]GTP (Hartmann Analytic, Germany) (33 nM, 6000 Ci mmol^{-1}). Fifteen microliters of this labeling mix were added to 15 μl of elongation mix containing 0.1 mg ml^{-1} heparin (Sigma) and the 4 NTP (0.5 mM final concentration) in the same buffer. Protein NusA from *E. coli* (0.3 μM final concentration) was added in the elongation mix when needed. The reaction was quenched with 150 μl of ethanol and Na-acetate 0.3 M, precipitated and the radioactive products were analyzed on 6 or 10% denaturing polyacrylamide gels. Gels were dried, exposed on imaging plates and scanned on a Bioimager Analyzer (Fuji Photo Film Co, Ltd). Images were processed with our own programs.

Quantification of hydroxyl radical footprinting experiments

We have developed our own program for gel quantification. Basically, the method in use is the same as that described in,[54,55] but has several specificities linked to automation (unpublished). The overall quality of our procedure is illustrated in Fig. SD-3E showing excellent correlation between the cleavage patterns obtained with the *ATthiC* riboswitch aptamer and its prediction from the crystal structure.[51]

Differentiating the kinetic models

The two possible kinetic models correspond to equations 1a,b (model #1) and 2a,b (model #2). The results obtained with *kinITC* were in favor of model #1 for *ECthiC*, but not sufficiently for a definite conclusion, and they did not significantly differentiate the 2 models for *ECthiM*. For *ATthiC, kinITC* turned out to be inapplicable in part due to *ATthiC* being a slow folding RNA below 30°C (hence a weak heat-power producer), which implied using too high RNA concentration to obtain sufficient signal-to-noise ratio. Furthermore, ITC revealed the existence of a minor RNA species undetected by the other methods (see SD-17A,C), which also contributed to the inapplicability of *kinITC* with *ATthiC*. We thus considered other methods to obtain a clearcut answer.

Although *kinITC* alone did not allow differentiating the 2 models convincingly for *ECthiC* and *ECthiM*, the kinetic parameters obtained with each model were quite different and we confronted the 2 sets of results with fully independent observations, either from our own experiments using •OH footprinting and Surface Plasmon Resonance (SPR), or from published fluorescence-based experiments.[23] The basis of the method is as follows.

We need to describe how the concentrations of the 3 RNA species (R_0, R_1, R_2 in equations 1-2) evolve after any perturbation, for example in our experimental systems after addition of TPP or, *in vivo*, immediately after synthesis of the aptamer in presence of TPP. In both cases the system evolves from an initial state ($t = 0$) with no TPP bound to the RNA, to the equilibrium state where the different concentrations of R_0, R_1, R_2 are defined by the equilibrium constants K_d and K_F. In situations where TPP is in large excess ($L_{tot} \gg R_{tot}$, L_{tot} and R_{tot} being the total TPP and RNA concentrations), as in •OH footprinting experiments, the kinetic equations describing the evolution of the concentrations can be linearized by assuming that $L(t) \approx L_{tot}$ remains constant, which corresponds to pseudo first-order kinetics (equations S8.1a,b in SD-8). In SPR experiments, the latter assumption is still valid due to continuous injection of TPP even though the bulk concentration of TPP may not be in large excess relative to the RNA. *In vivo*, the concentrations of the concerned mRNAs lie in the nanomolar, or high nanomolar range, that is well below the TPP concentration, and the same assumption $L(t) \approx$ constant is valid (of course, the TPP concentration is not constant during the life cycle of a cell, but its variation is on a longer time-scale than that necessary for the functioning of a riboswitch). As a consequence of this first-order approximation, classical calculations (see SD-8) show that the variations of the RNA concentrations from this initial state to equilibrium are given by:

$$R_i(t) = \tilde{R}_i + f_i exp(-k_{fast}t) + s_i exp(-k_{slow}t) \qquad (4)$$

with $i = 0,1,2$, $\tilde{R}_i$ the concentration of the ith RNA species at equilibrium (*i.e.*, that can be calculated from L_{tot} and the equilibrium constants K_d, K_F only: See equation S8.3b in SD-8), f_i, s_i being time independent coefficients specific for the species R_i, and k_{slow}, k_{fast} ($k_{slow} < k_{fast}$) being kinetic parameters governing, respectively, a 'slow' and a 'fast' component of concentration variations during the return to equilibrium.

Importantly, all these parameters depend only on k_{on}, k_{off}, k_F, k_U (equations 1, 2) and on L_{tot}. Note also that the appearance of a 'slow' and a 'fast' component and, thus, of 2 distinct time scales ($\tau_{short} = k_{fast}^{-1}$ and $\tau_{long} = k_{slow}^{-1}$), results naturally from the mathematical treatment of a 2-step mechanism in the frame of first-order approximation. The expressions for k_{slow} and k_{fast} can be obtained as (see,[56] pp. 118-119 and SD-8 for full details):

$$k_{fast \text{ or } slow} = \frac{1}{2}[k_U + k_F + k_{on}(L_{tot} + K_d)]$$

$$\left(1 \pm \sqrt{1 - \frac{4k_{on}k_U K_{model}}{[k_U + k_F + k_{on}(L_{tot} + K_d)]^2}}\right) \qquad (5a)$$

k_{fast} and k_{slow} corresponding, respectively, to the plus and minus sign within the parenthesis, and the term K_{model} being model-dependent according to:

$$K_{model\#1} = K_d + (1 + K_F)L_{tot} \qquad (5b)$$

$$K_{model\#2} = K_d + K_F(L_{tot} + K_d) \qquad (5c)$$

To get insight into a reaction mechanism it is common to monitor the kinetic effects resulting from the variation of L_{tot}. However, without using a particular experimental setup able to record short-time variations (or by voluntarily disregarding badly resolved short-time variations), only the slow kinetic component will show up (or will be used) in the experimental data, which explains the importance of the function $k_{slow}(L_{tot})$ (see SD-9 for a detailed discussion on $k_{slow}(L_{tot})$). Equations (4 and 5a-c) will be of great importance for establishing a quantitative model of kinetic regulation. These are also at the basis of the processing of •OH footprinting data to obtain information both on the primary site of TPP interaction and on the kinetics of TPP binding (see below 'Quantification of the kinetic curves from hydroxyl radical footprinting'). Equations (4, 5a-c) were also used to process the successive SPR binding curves acquired with increasing TPP concentrations by considering a 2-step mechanism.

Quantification of the kinetic curves from hydroxyl-radical footprinting

We used 2 different methods for processing the kinetic curves from •OH footprinting experiments with *ECthiC_{mutP1}* and *ATthiC*. These methods were particularly adapted to *ATthiC* due to its slow folding. The first method relied on a bi-exponential fit of each cleavage curve separately. Such a fit is justified by equation (4) since the evolution of all RNA concentrations, and thus of the cleavage of each species can be described by an equation of this type. This method allows obtaining values of $\tau_{short} = k_{fast}^{-1}$ and $\tau_{long} = k_{slow}^{-1}$ for each residue showing a clear cleavage signal. The second method sought to obtain more detailed information, both on the primary and secondary (or early and late) sites of TPP binding and on the kinetics of interaction. The essence of the method has been described in.[57] It consists in fitting the kinetic cleavage curves of all residues (apart for the badly resolved 5′ and 3′ ends) by

considering the evolution of the concentrations of the different RNA species following equation (4). The great difference with the previous method is that a global fit of all cleavage curves is performed at once, and not a separate fit for each curve. The great interest of this method is of yielding information on the cleavage propensity of each residue in all species R_0, R_1, R_2. All details are in SD-10.

Thermodynamic and kinetic information obtained with kinITC

The *kinITC* method has been described elsewhere.[22] We only recall here (i) that *kinITC* works by fitting simultaneously the complete shapes of all injection curves of several ITC experiments performed at different temperatures and (ii) that *kinITC* results are not obtained as discrete numerical values at these different temperatures but, instead, as explicit mathematical functions of the variation with the temperature of all thermodynamic and kinetic quantities. Importantly, *kinITC* is a model-dependent method that requires proposing a well-established kinetic description of the reaction(s) taking place after mixing of the reagents. Although related to the method described in,[58] it is more general, firstly because it does not disregard the short-time part of the injection curves potentially conveying information on a possible fast component and, secondly, because it can cope with situations involving 2 kinetic steps (equations 1a-b or 2a-b) to obtain thermodynamic and kinetic information about these 2 steps. This feature, unique to *kinITC*, was particularly important for the major result of this work about the kinetic regulation mechanism of such TPP riboswitches. Note that, in all ITC experiments, the TPP concentration is variable and a first-order approximation is inapplicable, which implies that the exact non-linear differential equations describing the kinetics of the reaction have to be integrated in *kinITC* processing.

For *ECthiC* and *ECthiM*, we used the method described for *ECthiC*$_{mutP1}$ in.[22] The temperatures were (20.2, 27, 27.3, 30, 34°C) for *ECthiC* and (18, 26, 30, 34, 37°C) for *ECthiM*. For each temperature, the initial RNA concentrations in the measurement cell were respectively: (24, 24, 21, 21, 21 μM) for *ECthiC* and (19.3, 18.8, 18.8, 18.8, 16.3 μM) for *ECthiM*, and the TPP concentrations in the syringe were 200 μM for *ECthiC* and (200, 200, 200, 200, 160 μM) for *ECthiM*.

Programming

Computer programs used in this work for gel processing, kinetic processing of $^\bullet$OH footprinting data, for SPR and *kinITC* experiments, as well as for illustrations (apart when indicated differently), were written with the *Mathematica* language from Wolfram Res. The symbolic capabilities of *Mathematica* were also of great interest throughout this work.

Disclosure of potential conflicts of interest

No potential conflicts of interest were disclosed.

References

1. Berg JM, Tymoczko JL, Stryer L. Biochemistry. New York: W.H. Freeman, 2002
2. Nakayama H, Hayashi R. Biosynthesis of thiamine pyrophosphate in Escherichia coli. J Bacteriol 1972; 109:936-8; PMID:4550824
3. Rodionov DA. Comparative genomics of thiamin biosynthesis in procaryotes. new genes and regulatory mechanisms. J Biol Chem 2002; 277:48949-59; PMID:12376536; http://dx.doi.org/10.1074/jbc.M208965200
4. Jurgenson CT, Begley TP, Ealick SE. The structural and biochemical foundations of thiamin biosynthesis. Annu Rev Biochem 2009; 78:569-603; PMID:19348578; http://dx.doi.org/10.1146/annurev.biochem.78.072407.102340
5. Miranda-Rios J. From the Cover: A conserved RNA structure (thi box) is involved in regulation of thiamin biosynthetic gene expression in bacteria. Proc Natl Acad Sci U S A 2001; 98:9736-41; PMID:11470904; http://dx.doi.org/10.1073/pnas.161168098
6. Winkler W, Nahvi A, Breaker RR. Thiamine derivatives bind messenger RNAs directly to regulate bacterial gene expression. Nature 2002; 419:952-6; PMID:12410317; http://dx.doi.org/10.1038/nature01145
7. Mironov AS, Gusarov I, Rafikov R, Lopez LE, Shatalin K, Kreneva RA, Perumov DA, Nudler E. Sensing small molecules by nascent RNA: a mechanism to control transcription in bacteria. Cell 2002; 111:747-56; PMID:12464185; http://dx.doi.org/10.1016/S0092-8674(02)01134-0
8. Nahvi A, Sudarsan N, Ebert MS, Zou X, Brown KL, Breaker RR. Genetic control by a metabolite binding mRNA. Chem Biol 2002; 9:1043; PMID:12323379; http://dx.doi.org/10.1016/S1074-5521(02)00224-7
9. Nou X, Kadner RJ. Adenosylcobalamin inhibits ribosome binding to btuB RNA. Proc Natl Acad Sci U S A 2000; 97:7190-5; PMID:10852957; http://dx.doi.org/10.1073/pnas.130013897
10. Ravnum S, Andersson DI. Vitamin B12 repression of the btuB gene in Salmonella typhimurium is mediated via a translational control which requires leader and coding sequences. Mol Microbiol 1997; 23:35-42; PMID:9004218; http://dx.doi.org/10.1046/j.1365-2958.1997.1761543.x
11. Roth A, Breaker RR. The structural and functional diversity of metabolite-binding riboswitches. Annu Rev Biochem 2009; 78:305-34; PMID:19298181; http://dx.doi.org/10.1146/annurev.biochem.78.070507.135656
12. Wachter A, Tunc-Ozdemir M, Grove BC, Green PJ, Shintani DK, Breaker RR. Riboswitch Control of Gene Expression in Plants by Splicing and Alternative 3′ End Processing of mRNAs. Plant Cell Online 2007; 19:3437-50; PMID:17993623; http://dx.doi.org/10.1105/tpc.107.053645
13. Barrick JE, Breaker RR. The distributions, mechanisms, and structures of metabolite-binding riboswitches. Genome Biol 2007; 8:R239; PMID:17997835; http://dx.doi.org/10.1186/gb-2007-8-11-r239
14. Garst AD, Edwards AL, Batey RT. Riboswitches: structures and mechanisms. Cold Spring Harb Perspect Biol 2011; 3; PMID:20943759; http://dx.doi.org/10.1101/cshperspect.a003533
15. Serganov A, Patel DJ. Molecular recognition and function of riboswitches. Curr Op Struct Biol 2012; 22:279-86; PMID:22579413; http://dx.doi.org/10.1016/j.sbi.2012.04.005

16. Serganov A, Nudler E. A decade of riboswitches. Cell 2013; 152:17-24; PMID:23332744; http://dx.doi.org/10.1016/j.cell.2012.12.024

17. Wickiser JK, Cheah MT, Breaker RR, Crothers DM. The kinetics of ligand binding by an adenine-sensing riboswitch. Biochemistry 2005; 44:13404-14; PMID:16201765; http://dx.doi.org/10.1021/bi051008u

18. Wickiser JK, Winkler WC, Breaker RR, Crothers DM. The speed of RNA transcription and metabolite binding kinetics operate an FMN riboswitch. Mol Cell 2005; 18:49-60; PMID:15808508; http://dx.doi.org/10.1016/j.molcel.2005.02.032

19. Kawasaki T, Miyata I, Esaki K, Nose Y. Thiamine uptake in Escherichia coli. I. General properties of thiamine uptake system in Escherichia coli. Arch Biochem Biophys 1969; 131:223-30; PMID:4889357; http://dx.doi.org/10.1016/0003-9861(69)90125-8

20. Leonardi R, Roach PL. Thiamine biosynthesis in Escherichia coli: in vitro reconstitution of the thiazole synthase activity. J Biol Chem 2004; 279:17054-62; PMID:14757766; http://dx.doi.org/10.1074/jbc.M312714200

21. Ontiveros-Palacios N, Smith AM, Grundy FJ, Soberon M, Henkin TM, Miranda-Rios J. Molecular basis of gene regulation by the THI-box riboswitch. Mol Microbiol 2008; 67:793-803; PMID:18179415; http://dx.doi.org/10.1111/j.1365-2958.2007.06088.x

22. Burnouf D, Ennifar E, Guedich S, Puffer B, Hoffmann G, Bec G, Disdier F, Baltzinger M, Dumas P. kinITC: a new method for obtaining joint thermodynamic and kinetic data by isothermal titration calorimetry. J Am Chem Soc 2012; 134:559-65; PMID:22126339; http://dx.doi.org/10.1021/ja209057d

23. Lang K, Rieder R, Micura R. Ligand-induced folding of the thiM TPP riboswitch investigated by a structure-based fluorescence spectroscopic approach. Nucleic Acids Res 2007; 35:5370-8; PMID:17693433; http://dx.doi.org/10.1093/nar/gkm580

24. Kulshina N, Edwards TE, Ferre-D'Amare AR. Thermodynamic analysis of ligand binding and ligand binding-induced tertiary structure formation by the thiamine pyrophosphate riboswitch. RNA 2009; 16:186-96; PMID:19948769; http://dx.doi.org/10.1261/rna.1847310

25. Edwards TE, Klein DJ, Ferré-D'Amaré AR. Riboswitches: small-molecule recognition by gene regulatory RNAs. Current Op Struct Biol 2007; 17:273-9; PMID:17574837; http://dx.doi.org/10.1016/j.sbi.2007.05.004

26. Mortimer SA, Weeks KM. C2′-endo nucleotides as molecular timers suggested by the folding of an RNA domain. Proc Natl Acad Sci U S A 2009; 106:15622-7; PMID:19717440; http://dx.doi.org/10.1073/pnas.0901319106

27. Haller A, Altman RB, Souliere MF, Blanchard SC, Micura R. Folding and ligand recognition of the TPP riboswitch aptamer at single-molecule resolution. Proc Natl Acad Sci U S A 2013; 110:4188-93; PMID:23440214; http://dx.doi.org/10.1073/pnas.1218062110

28. Anthony PC, Perez CF, Garcia-Garcia C, Block SM. Folding energy landscape of the thiamine pyrophosphate riboswitch aptamer. Proc Natl Acad Sci U S A 2012; 109:1485-9; PMID:22219369; http://dx.doi.org/10.1073/pnas.1115045109

29. Garst AD, Batey RT. A switch in time: detailing the life of a riboswitch. Biochim Biophys Acta 2009; 1789:584-91; PMID:19595806; http://dx.doi.org/10.1016/j.bbagrm.2009.06.004

30. Rentmeister A, Mayer G, Kuhn N, Famulok M. Conformational changes in the expression domain of the Escherichia coli thiM riboswitch. Nucleic Acids Res 2007; 35:3713-22; PMID:17517779; http://dx.doi.org/10.1093/nar/gkm300

31. Warner KD, Homan P, Weeks KM, Smith AG, Abell C, Ferre-D'Amare AR. Validating fragment-based drug discovery for biological RNAs: lead fragments bind and remodel the TPP riboswitch specifically. Chem Biol 2014; 21:591-5; PMID:24768306; http://dx.doi.org/10.1016/j.chembiol.2014.03.007

32. Edwards TE, Ferré-D'Amaré AR. Crystal Structures of the Thi-Box Riboswitch Bound to Thiamine Pyrophosphate Analogs Reveal Adaptive RNA-Small Molecule Recognition. Structure 2006; 14:1459-68; PMID:16962976; http://dx.doi.org/10.1016/j.str.2006.07.008

33. Cressina E, Chen L, Moulin M, Leeper FJ, Abell C, Smith AG. Identification of novel ligands for thiamine pyrophosphate (TPP) riboswitches. Biochem Soc Trans 2011; 39:652-7; PMID:21428956; http://dx.doi.org/10.1042/BST0390652

34. Beisel CL, Smolke CD. Design principles for riboswitch function. PLoS Comput Biol 2009; 5:e1000363; PMID:19381267; http://dx.doi.org/10.1371/journal.pcbi.1000363

35. Perdrizet GA, 2nd, Artsimovitch I, Furman R, Sosnick TR, Pan T. Transcriptional pausing coordinates folding of the aptamer domain and the expression platform of a riboswitch. Proc Natl Acad Sci U S A 2014; 109:3323-8; PMID:22331895; http://dx.doi.org/10.1073/pnas.1113086109

36. Holmstrom ED, Polaski JT, Batey RT, Nesbitt DJ. Single-molecule conformational dynamics of a biologically functional hydroxocobalamin riboswitch. J Am Chem Soc 2014; 136:16832-43; PMID:25325398; http://dx.doi.org/10.1021/ja5076184

37. Mishler DM, Gallivan JP. A family of synthetic riboswitches adopts a kinetic trapping mechanism. Nucleic Acids Res 2014; 42:6753-61; PMID:24782524; http://dx.doi.org/10.1093/nar/gku262

38. Toulokhonov I, Landick R. The flap domain is required for pause RNA hairpin inhibition of catalysis by RNA polymerase and can modulate intrinsic termination. Mol Cell 2003; 12:1125-36; PMID:14636572; http://dx.doi.org/10.1016/S1097-2765(03)00439-8

39. Artsimovitch I, Landick R. Pausing by bacterial RNA polymerase is mediated by mechanistically distinct classes of signals. Proc Natl Acad Sci U S A 2000; 97:7090-5; PMID:10860976; http://dx.doi.org/10.1073/pnas.97.13.7090

40. Pan T, Artsimovitch I, Fang XW, Landick R, Sosnick TR. Folding of a large ribozyme during transcription and the effect of the elongation factor NusA. Proc Natl Acad Sci U S A 1999; 96:9545-50; PMID:10449729; http://dx.doi.org/10.1073/pnas.96.17.9545

41. Wong TN, Pan T. RNA folding during transcription: protocols and studies. Methods Enzymol 2009; 468:167-93; PMID:20946770; http://dx.doi.org/10.1016/S0076-6879(09)68009-5

42. Bocobza S, Adato A, Mandel T, Shapira M, Nudler E, Aharoni A. Riboswitch-dependent gene regulation and its evolution in the plant kingdom. Genes Dev 2007; 21:2874-9; PMID:18006684; http://dx.doi.org/10.1101/gad.443907

43. Pose D, Verhage L, Ott F, Yant L, Mathieu J, Angenent GC, Immink RG, Schmid M. Temperature-dependent regulation of flowering by antagonistic FLM variants. Nature 2013; 503:414-7; PMID:24067612; http://dx.doi.org/10.1038/nature12633

44. Tomsic J, McDaniel BA, Grundy FJ, Henkin TM. Natural variability in S-adenosylmethionine (SAM)-dependent riboswitches: S-box elements in bacillus subtilis exhibit differential sensitivity to SAM In vivo and in vitro. J Bacteriol 2008; 190:823-33; PMID:18039762; http://dx.doi.org/10.1128/JB.01034-07

45. Burmann BM, Rosch P. The role of E. coli Nus-factors in transcription regulation and transcription:translation coupling: From structure to mechanism. Transcription 2011; 2:130-4; PMID:21922055; http://dx.doi.org/10.4161/trns.2.3.15671

46. Lünse CE, Scott FJ, Suckling CJ, Mayer G. Novel TPP-riboswitch activators bypass metabolic enzyme dependency. Frontiers Chem 2014; 2:1-8; PMID:21615107; http://dx.doi.org/10.3389/fchem.2014.00053

47. Blouin S, Mulhbacher J, Penedo JC, Lafontaine DA. Riboswitches: ancient and promising genetic regulators. Chem Bio Chem 2009; 10:400-16; PMID:19101979; http://dx.doi.org/10.1002/cbic.200800593

48. Deigan KE, Ferré'd'Amaré AR. Riboswitches: discovery of drugs that target bacterial gene-regulatory RNAs. Acc Chem Res 2011; 44:1329-38; PMID:21615107; http://dx.doi.org/10.1021/ar200039b

49. Thore S, Frick C, Ban N. Structural basis of thiamine pyrophosphate analogues binding to the eukaryotic riboswitch. J Am Chem Soc 2008; 130:8116-7; PMID:18533652; http://dx.doi.org/10.1021/ja801708e

50. Walker SC, Avis JM, Conn GL. General plasmids for producing RNA in vitro transcripts with homogeneous ends. Nucleic Acids Res 2003; 31:e82; PMID:12888534; http://dx.doi.org/10.1093/nar/gng082

51. Thore S, Leibundgut M, Ban N. Structure of the eukaryotic thiamine pyrophosphate riboswitch with its regulatory ligand. Science 2006; 312:1208-11; PMID:16675665; http://dx.doi.org/10.1126/science.1128451

52. Shcherbakova I, Mitra S, Beer RH, Brenowitz M. Fast Fenton footprinting: a laboratory-based method for the time-resolved analysis of

DNA, RNA and proteins. Nucleic Acids Res 2006; 34:e48; PMID:16582097; http://dx.doi.org/10.1093/nar/gkl055

53. Karlsson R, Katsamba PS, Nordin H, Pol E, Myszka DG. Analyzing a kinetic titration series using affinity biosensors. Anal Biochem 2006; 349:136-47; PMID:16337141; http://dx.doi.org/10.1016/j.ab.2005. 09.034

54. Das R, Laederach A, Pearlman SM, Herschlag D, Altman RB. SAFA: semi-automated footprinting analysis software for high-throughput quantification of nucleic acid footprinting experiments. RNA 2005; 11:344-54; PMID:15701734; http://dx.doi.org/ 10.1261/rna.7214405

55. Laederach A, Das R, Vicens Q, Pearlman SM, Brenowitz M, Herschlag D, Altman RB. Semiautomated and rapid quantification of nucleic

acid footprinting and structure mapping experiments. Nature Protoc 2008; 3:1395-401; http://dx.doi.org/10.1038/nprot.2008.134

56. Fersht A. Enzyme structure and mechanism. Reading & San Franciso: Freeman WH, Co., 1977

57. Martin JS, Simmons K, Laederach A. Exhaustive Enumeration of Kinetic Model Topologies for the Analysis of Time-Resolved RNA Folding. Algorithms 2009; 2:200-14; PMID:19865589; http://dx.doi. org/10.3390/a2010200

58. Vander Meulen KA, Butcher SE. Characterization of the kinetic and thermodynamic landscape of RNA folding using a novel application of isothermal titration calorimetry. Nucleic Acids Res 2012; 40:2140-51; PMID:22058128; http://dx.doi.org/10.1093/nar/ gkr894